Hygrothermal performance evaluation of traditional brick masonry in historic buildings

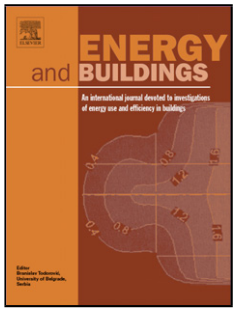

Title: Hygrothermal performance evaluation of traditional brick masonry in historic buildings

Author: Giovanni Litti Somayeh Khoshdel Amaryllis Audenaert Johan Braet

PII: S0378-7788(15)30165-1
DOI: http://dx.doi.org/doi:10.1016/j.enbuild.2015.07.049
Reference: ENB 6043

To appear in: *ENB*

Received date: 7-2-2015
Revised date: 22-6-2015
Accepted date: 20-7-2015

Please cite this article as: G. Litti, S. Khoshdel, A. Audenaert, J. Braet, Hygrothermal performance evaluation of traditional brick masonry in historic buildings, *Energy and Buildings* (2015), http://dx.doi.org/10.1016/j.enbuild.2015.07.049

Hygrothermal performance evaluation of traditional brick masonry in historic buildings

Giovanni Litti* (1)
Somayeh Khoshdel (1)
Amaryllis Audenaert (1)(2)
Johan Braet (2)

(1) EMIB Lab, Applied Engineering Laboratory for Sustainable Materials, Infrastructures and Buildings, Antwerp University; Campus Paardenmarkt; Rodestraat 4, 2000 Antwerp (Belgium)
(2) Department Engineering Management, Antwerp University; City Campus; Prinsstraat 13, 2000 Antwerp (Belgium)

* Corresponding author. Tel 0032 032137934; E-mail adress: giovanni.litti@uantwerpen.be

ABSTRACT

Existing buildings account for 40% of total green gas emission in the atmosphere [1][2]. Historic and heritage buildings are part of this building stock, and the need for improving their energy performance, despite the derogations for officially protected ones, is supported for achieving the European 2020 Energy Strategy aims [3].
However, when dealing with these buildings, not only are the intervention measures constrained by possible architectural preservation requirements, but also the preparatory building diagnosis itself: only non-destructive and non-invasive monitoring techniques are, reasonably, allowed. Therefore, during onsite energy auditing, ad-hoc monitoring protocols should be adopted.
In this study, an indirect non-invasive envelope monitoring, for evaluating brick masonry hygrothermal behavior, has been proposed and applied in a heritage building in Antwerp (Belgium). The suggested method is aimed at onsite evaluating the thermal performance of buildings traditional masonry and at quantifying the extent of its alteration due to the moisture distribution variation.
Areas detected as wet during iterative passive infrared thermography and environmental monitoring, showed thermal transmittance values more than three times higher than the dry ones on the same masonry surface.

KEY WORDS

Indirect hygrothermal performance analysis; indoor climate monitoring; IRT; *in-situ* thermal transmittance value measurement; moisture detection; historic buildings

1. DEFINITIONS AND ABBREVIATIONS

- *Notional and experimental data*; the authors refer to notional data (e.g, physical characteristics) when these are Standard-based calculated or simulated as defined by Fokaides et. al. in [4] and to *experimental data* when these are *in-situ* or in lab measured (e.g. thermal conductance according to the EN 9869) [5].
- *Historic building*; the authors refer to historic buildings when these have documented historic and/or architectural interest; see Art 1, comma 1-2 in [6].
- *NDT*; Non-Destructive Technology
- *IRT*; InfraRed Thermography
- *Quasi in contact hygrothermal parameters;* the authors refer to quasi in contact hygrothermal parameters when the physical quantities are measured quasi in contact with a given envelope surface, in [7].
- *Thermal inhomogeneous layers;* the authors refer to thermal inhomogeneous layers as the opposite of *homogeneous layer*, defined in EN ISO 6946; *Section 3 Terms and definitions*. The building components with inhomogeneous layers, such as mixed stone-mortar masonry or double brick leaf with central filled cavity masonry, cannot be calculated by following the procedure in 6.2.2- 6.2.5; *Section 6 Total thermal Resistance*; EN ISO 6946 [8].

1.1 NOMENCALTURE

- *(T)*; Air Dry Bulb Temperature (°C)
- (T_{dw}); Dew Point Temperature (°C)
- *(RH)*; Relative Humidity (%)
- *(MR);* Air Mixing Ratio (g/kg)
- *(EMC)*; Equilibrium Moisture Content (%)
- *(q)*; Density of heat flow rate (W/m^2)
- *(U);* Thermal transmittance (W/m^{2}K)
- (R_{si}); Internal surface thermal resistance (m^{2}K/W)
- (R_{se}); External surface thermal resistance (m^{2}K/W)
- *(R)*; Thermal Resistance (m^{2}K/W)
- *(λ);* Thermal conductivity (W/mK)
- *(Λ);* Thermal conductance (W/m^{2}K)
- (h_i); Internal surface film coefficient for heat transfer (W/m^{2}K)
- (h_e); External surface film coefficient for heat transfer (W/m^{2}K)
- *(Θsi)* Surface temperature indoor (°C)
- *(Θse)* Surface temperature outdoor (°C)
- *(ω);* Material moisture content by weight (%)
- ($\Theta_{si\,min}$); Minimum surface temperature indoor (°C)
- ($\Theta_{si\,max}$); Maximum surface temperature indoor (°C)
- *(σΘs);* Mean surface temperature indoor (°C)
- *(Θsi);* Surface temperature on the point (°C)
- *(Θi);* Air indoor temperature (°C)
- *(Θe);* Air outdoor temperature (°C)
- *(σΘi);* Mean air indoor temperature (°C)
- *(σΘe);* Mean air outdoor temperature (°C)
- (Θ_d); Indoor dew point temperature (°C)
- (μ_s); Surface temperature factor (-)
- (μ_{sm}); Minimum surface temperature factor (-)
- (μ_s^*); Modified surface temperature factor (-)
- (μ_h); Heterogeneity surface temperature factor (-)
- (Δ_T); Temperature gradient indoor-outdoor of the dry bulb air temperature (°C)

2. INTRODUCTION

Existing buildings in Europe account for 40% of total green gas emissions in atmosphere. The urgency upon their energy refurbishment is, hence, agreed and economically sponsored by the EU State Members [1][2]. The attention in reducing building energy demand is currently increasing also with regard to historic and heritage buildings [3].

Since, in these buildings, heat losses through opaque components produce the highest impact on the overall energy balance [9], internal or external masonry insulation has been considered, for some time now, a consolidated retrofitting praxis.

However, when implementing such techniques in historic buildings, their effectiveness should be assured either considering the materials' compatibility or the long term variation of the existing masonry hygrothermal behaviour [10][11][12]. A preliminary onsite monitoring activity for quantifying the hygrothermal masonry performance in its current state, is fundamental.

Therefore, not only should the retrofitting strategy be considered non-harmful for the building, but also the preliminary diagnosis itself. This poses a serious scientific and methodological problem as several monitoring techniques cannot be implemented in historic and heritage contexts due to their invasiveness.

The problem cannot be avoided by simply neglecting preliminary onsite measurement campaigns. Indeed, due to the heterogeneous and anisotropic masonry behaviour, alongside with local deterioration processes (responsible for material physical properties variations), the masonry hygrothermal dynamics need to be verified in their current conditions. Experimental onsite monitoring and successive laboratory analysis are thus strongly recommended as opposed to mere notional calculations. However, due to the aforementioned constraints imposed by preservation requirements, often only indirect assessment methodologies are implementable [13][14][15].

In this contribution, a description of possible hygrothermal envelope-assessment inaccuracies, increased as a consequence of lack of onsite monitoring campaigns, as well as methodological problems encountered in the current praxis are discussed in section 3. Moreover, an overview on current standards and instrumental monitoring methodologies for opaque components hygrothermal performance evaluation is given in sections 4 and 5.

Finally, an indirect monitoring methodology aimed at evaluating masonry thermal performance and its variation according to moisture distribution is discussed in section 6.

The methodology implemented in Vleeshuis Museum in Antwerp is described in section 7, obtained results are discussed in section 8, while conclusion are drawn in section 9.

Although this contribution focuses on the results of a specific case study, the described monitoring procedure can be applied in cases in which the preparatory diagnosis to the building refurbishment is limited by preservation building requirements.

3. BUILDING OPAQUE COMPONENTS THERMAL EVALUATION: TECHNICAL AND METHODOLOGICAL PROBLEMS FOR ITS DEFINITION

Since opaque components (especially walls) account for the most extensive envelope surface in historic buildings [9], their correct thermal performance evaluation is fundamental for delivering effective retrofitting strategies.

The lack of onsite thermal component evaluation, such as in case of analyses solely based on standardised or notional data, might result either in inaccurate or unrepresentative building envelope evaluations or even in improper intervention proposals [16].

In this paragraph, an overview of the widely reported causes of discrepancy between experimental and notional calculated or simulated thermal performance (expressed by the U value) of existing building opaque partitions is given.

Although the reported issues refer mainly to buildings masonry, few of them have been encountered during different materials or components evaluation. The mentioned discrepancies are generally caused by the lack of knowledge on:

a) Component inhomogeneities or inner geometric discontinuities (e.g. materials decay, cracks);
b) Exact materials stratigraphy, percentage of mortar, eventual consistency of filled cavities;
c) Dynamic effect of moisture distribution into the masonry or part thereof;

Differences up to 30%, between experimental and notional U values in cavity and timber frame walls were found by S. Doran as a consequence of construction defects not predictable within the calculations [17]. The same percentage of deviation between calculated and measured U values, caused by a lack of information on hygrometric material properties and percentage of used materials[1], was found by P. Baker while investigating thermal properties of construction elements in traditional Scottish buildings [18]. The results from the study demonstrated that 44% of the measured walls had U value lower than the calculated or simulated one, 42% of the measured U values were in compliance with the values from the computations and only 8% of the measured walls had U values higher than the simulated or calculated ones. The potential sources of uncertainty referred by the author were mainly ascribable to the lack of detailed information on: wall stratigraphy, ratio and typology of stones and mortar, wall cavities and specific thermal properties of materials.
Onsite building monitoring, together with laboratory and numerical analyses, aimed at evidencing the extent of energy losses through envelope irregularities and thermal bridges[2] were discussed by Asdrubali et al. in [19], by Albatici et al. in [20] and by Fokaides in [4].
Generally within the mentioned studies, especially when related to masonry in historic buildings, the aspects below were highlighted:

- Overestimation of U values when calculated with commercial software if compared to the experimental diagnosis results.
- Underestimation of traditional masonry thermal performance within currently used guidelines, such as EST or CISBE[3].

Beside the points a) and b), also the dynamic effect of moisture or water (or, more rarely, ice) has to be considered as an additional driving cause of deviation between notional and experimental U values into historic masonry (or opaque component).
Since water has higher specific heat (5 times more) and higher thermal conductivity (20-22 times more) than common building materials, its presence in the building envelope, may locally or globally modify the thermal behaviour of the latter one[4]. Nevertheless, moisture not only affects masonry thermal performance, but also life span of used retrofitting materials; especially if hygroscopic, such as the ones that should be preferred in historic buildings.
The underestimation of the presence, distribution and movement of moisture when evaluating the thermal performance of envelope components, may decrease or nullify the effectiveness of the designed envelope insulation strategy[5]. It might also lead to the speedup of material decay and the increase of both risk of economic and energy losses [21] and architectural threat to the building and to its indoor microclimate quality [22][23][11][24].
Studies on the influence of moisture exchange of retrofitted walls and on the indoor relative humidity fluctuations have been published by C. Ferreira in [25], while studies on the relation between the envelope hygrothermal behavior and the building's microclimate were published by Camuffo et.al. in [26][27].
By performing laboratory measurements on thermal conductivity of brick samples, S. R. Duverne and P. Backer delivered results with a strong correspondence between experimental and notional masonry thermal transmittance values. This was allowed by considering the physical relation between hygrometric and thermal materials properties of the investigated traditional masonry materials [28]. The authors documented the high correlation between materials moisture content by weight (ω) and thermal conductivity (λ). The capillary moisture content increase after wetting the material samples, caused a thermal conductivity

[1] Percentage of used material such as brick-mortar ratio; See *Conclusion*; p. 31 in [18]
[2] Material, geometrical and structural thermal bridges; as defined by E. Lucchi in [58]
[3] Paragraph 5.6 Comparison to often quoted used U values, pp. 27-28 in [18]
[4] Surfaces interested by water absorption may have altered thermal transmittance value due to the local thermal conductivity increase.
[5] Wet insulation materials (increased MC) have reduced efficacy (increased effective λ) independently from their density in [65]

increase up to 3 times more than the dry material thermal conductivity; therefore, during the calculations, the authors considered a twofold λ value for materials in dry and wet state[6].

A similar linear correlation, although with a lower slope, was found by Pavlikova' et al., with regard to load bearing structural materials [29]. In the study, *U* value was measured on materials in their dry and wet state[7]. A high convergence between measured and calculated masonry *U* values was achieved when simulations were performed considering range of theoretical thermal conductivity variation[8], instead of a unique given standard material (dry) λ value.

Further studies on the influence of moisture content increase on thermal conductivity variation (considering yearly cycles) were conducted by R.N.M. Ramons et al in [24]. Within the study, commercial hygrothermal simulation software[9] were compared for assessing the hygrothermal performance of thermal insulation panels and walls structures. In the study, the sharp λ increase during typical winter weather conditions was described: in winter, insulation panel thermal conductivity rose due to the material moisture content increase, while it decreased again in summer when the moisture content was lowered by the material natural drying. Therefore, it occurs that, when insulation panels should ensure the highest thermal performance, the insulation efficiency is lowered by the moisture increase. This condition is often neglected during envelope retrofitting design causing premature insulating panel decay. Not only vapour or water barriers are sufficient for avoiding insulation panel dampness, but also the dryness of the masonry itself. Furthermore the choice of preferring hydrophobic insulation panels on hygroscopic traditional materials should open a discussion on the significance of retrofit sustainability [10].

The effect of hygrothermal behaviour variation over the time in a traditional masonry, before and after the application of insulation layers, was also studied by R. Hendrickx et al. in [11]. The study concluded that the investigated masonry, without insulation, was able to dry completely during the spring-summer drying cycles, but after the application of 12cm calcium silicate layer the wall core experienced a moisture content increase impossible to be reduced by the natural seasonal cycles.

A similar study on the hygrothermal consequences of improper insulated masonry was proposed by D. Brouwne in [30]. Within the study, moisture failure was predicted on the outer layer of the vapour barrier in internally insulated walls[10].

Beside the long term seasonal cycles variations, the thermal conductivity increase may occur temporary, in specific environmental conditions. The increase of thermal conductivity (λ) due to driven rain is reported by F. Ochs et al. in [31]. The time shift in which the material regains its nominal physical properties (after the drying cycle) is also investigated. The authors pointed out the importance of considering the temperature increase as second driving factor causing thermal transmittance value fluctuations. Moisture transport is temperature-dependent; moreover, the thermal conductivity increases significantly with both moisture content and temperature increase. The relation function between specific heat capacity and moisture content, based on the linear combination of volumetric heat capacity of both dry and wet insulation panel specimens and the moisture content (MC), was studied for different insulation panels by M. Jerman et al. in [32].

Beside the above described discrepancies between experimental and notional components thermal performance, mainly caused by the lack of knowledge in the current technological characteristics or by inappropriate calculation assumptions [30], it also happens that, despite a good knowledge on e.g. masonry stratigraphy as well as localised inhomogeneities or moisture distribution variations, there is no possibility of a direct integration of these information within the envelope thermal performance assessment model. Due to the widely reported limitations within the Standard-based calculation procedures[11] [33][9], the local masonry properties variations (caused by e.g. cracking and infiltration or capillarity), although known, are anyhow neglected in favor of a unique representative thermal transmittance value measured and/or calculated. This causes dangerous simplifications both at the diagnosis and at the design level.

[6] See Figure 4a & 4b p. 26 in [28]
[7] The thermal conductivity in wet and dry conditions was measured at 10°C; Table 4; p. 32 in [28]
[8] Thermal transmittance value obtained by Standard but with range of variation from material dry state to material wet state.
[9] The software used by the authors were: Condensa 13788 and Wufi 5.0; Paragraph 2.2 Numerical results; p. 106 in [24]
[10] The moisture failure, in terms of masonry MC increase, was observed in the masonry layer in touch with the vapour barrier; p. 71; in [30]
[11] Constraints related to computational or simulation models, have been frequently posed in literature and are discussed in Section 4.

The above presented outline should not be meant either exhaustive of all the potential causes hampering the closeness between experimental and notional results, or indicative of all the problematics included within the current Standard-based envelope thermal performance calculation procedures (see section 4), but it has to be considered as an overview of the most encountered methodological constrains either in scientific literature or in the technical praxis.

4. STANDARD OVERVIEW

In literature, several methods for *in-situ* measuring and calculating the thermal transmittance of traditional walls are proposed [34][35][28][36][19]. In case of historic buildings, due to their technological complexity and material deterioration heterogeneity, the measurement and successive calculation of the *U* value requires more accurate instrumental investigations than the ones regarding contemporary buildings[12]. In this paragraph, a general outline on the current standards aimed at the U value calculation or measurement, is presented.

According to the current European Technical Standards, the opaque component thermal transmittance value (*U*) can be calculated by knowing the components' stratigraphy and material properties (EN 6946) or directly *in-situ* measuring the component thermal conductance and thermal resistance (ISO 9869). The last procedure is not intended to replace the laboratory scale measurements, such as calorimeter and hot boxes, but it might be implemented if laboratory scale or destructive measurements are not allowed. This latter condition fits well in case of historic buildings.

The standard generally used for calculating the *U* value of opaque building components is the EN ISO 6946 [37][38]. Within the calculation procedure, accurate knowledge of the building component stratigraphy, material physical properties and boundary conditions are required[13]. Due to this, the standard does not apply straightforward to historic buildings where material information are not always available; moreover, as already mentioned in Sect. 3, the standard does not consider moisture-related phenomena despite their influence on the *U* value variation [37].

If a lack of material information occurs, the EN 6946 refers to EN ISO 10456 and EN ISO 7345. However, the mentioned two standards are only valid for present-day materials and construction techniques.

In case of solid masonry, the thermal conductivity can be determined either from in-situ tests or from tabular data. To provide notional data, the EN 1745 delivers dry thermal conductivity of clay bricks at average temperature of 10°C. Other characteristics such as: water vapour diffusion, specific heat and moisture coefficient (which describes the increase of λ per percentage increase of moisture content)[14] are also delivered. Nonetheless, as the mentioned tabulated parameters are density-related, this tabular data can be used only if during the material production there has been density control. Obviously this requirement is again not suitable for historic buildings.

The second common methodology for obtaining the thermal transmittance of walls, implemented within this research, is the in-situ heat flux metering. The ISO 9869 proposes guidelines for in-situ measuring the thermal conductance and thermal transmittance value of building opaque components.

This standard, in addition to provide the measurement methodology, delivers recommendations on the equipment to be used and the data processing procedures taking into account parameters variability and monitoring uncertainties.

5. TECHNIQUES FOR MOISTURE DIAGNOSIS

In this Section, the most employed onsite non-destructive techniques (NDT) used for moisture detection are reviewed.

Here Table 5.1

[12] For which the homogeneity assumption is more applicable.

[13] Such as: thermal conductivity, vapour pressure resistance or other physical properties generally gettable from the material certifications.

[14] See Table A.1 in Annex 1; Tabulated $(\lambda_{10,dry})$ values of materials used for masonry products and mortar products; pp 17; in EN 1745 [66]

5.1 Infrared Thermography (IRT)

Infrared thermography is an indirect method widely employed also in historic buildings for thermal buildings diagnosis and moisture detection in the near surface region. This NDT is based on the measurement of the radiant thermal energy distribution which is emitted from a target by using an Infrared camera [39]. The camera is therefore not sensitive to water content but to temperature variation caused (also) by moisture presence in the masonry. This technique provides a map of surface temperature distribution[15] which can be directly related to moisture presence and variation [40][41][42].
Most of the researches indicate that IRT techniques provide a qualitative assessment of moisture distribution on the surface of historic masonry walls. However, several applications for enabling a quantitative assessment, providing useful information especially in case of cultural heritage, are published [43][19].
Currently, due to the lack of standardized protocol for MC *in-situ* assessment, IRT technique can only deliver a qualitative assessment of moisture distribution onto the masonry[16]. It is worth mentioning that IRT is strongly affected by environmental conditions, therefore in case of high relative humidity and low temperatures the outcomes are not always reliable[17] [44][45].

5.2 Nuclear Magnetic Resonance (NMR)

Nuclear Magnetic Resonance (NMR) is a non-invasive method for *in-situ* mapping and evaluating the quantitative distribution of moisture content in the first layers of a historic masonry[18].
NMR is based on the application of a magnetic field on one side of the wall; the hydrogen atoms are excited by pulse of radio frequency waves range, then the waves relax back to their normal state releasing a characteristic signal.
Measurement of the relaxation signal allows the understanding of present hydrogen atoms; with appropriate calibration for the specific material, the absolute water content can be evaluated [46]. Data obtained with NMR can be represented as a contour plot of absolute water content. This technique cannot be used in presence of iron nails and/or iron elements inside the masonry [44].

5.3 Holographic Radar

The holographic radar technique is a non-invasive technology which can provide qualitative measurement of water content in the depth range of 50- 200 mm beneath the surface as well as information about the texture of the wall, presence of cavities and detachment as function of operating continuous wave frequency. Due to the high dielectric permittivity of water, areas with increased level of moisture have high contrast on the result map. This technique is mainly not influenced by relative humidity or air temperature [44][47][48].
The output of this radar is a high spatial resolution image which is an amplitude modulated by the phase variation due to different subsurface electromagnetic properties of the investigated material [48][49]. To obtain reliable measurements, the measured surface should be flat so as to allow close and continuous contact with [49].

5.4 Ultrasonic

[15] Thermal image: Image produced by an infrared radiation sensing system and which represents the apparent radiance temperature distribution over a surface; in Definition; pp 5; NBN EN 13187 [39]
[16] A standard for the MC measurement on cultural heritage material is under approval by CEN/TC 346 prEN16682; Conservation of Cultural Heritage - Guide to the measurements of moisture content in materials constituting movable and immovable cultural heritage; moreover a Standard on thermal irregularities detection by IRT method is under development by the CEN/TC 163 pr EN 6781-2; Performance of buildings - Detection of heat, air and moisture irregularities in buildings by infrared methods - Part 2: Equipment Requirements.
[17] The IRT reliability increases if favorable environmental conditions: beside the advices within the EN 13187 [39], indoor hygrothermal conditions to be full filled during IRT moisture detection are proposed by Rosina et. al. in [45]. Indoor Relative Humidity lower than 70% and Indoor Air Temperature higher than 6-7°C
[18] NMR measures the amount of moisture in different physical states (i.e. chemically bound, physically bound and free liquid); in [46]

The ultrasonic test is a non-invasive method often applied to cultural heritage in order to detect surface and subsurface flaws or discontinuities in components and materials. This technique is mostly implemented within wood investigation [50][51].
The ultrasonic method is based on the property of sound or ultrasound waves transmitted through solid materials. The ultrasound velocity decreases as the moisture content increases.
During the ultrasonic measurement, unpredictable uncertainties are generated by structural discontinuities or in-homogeneities (e.g. fractures, changes in density, grain orientation, insect or mould) inside the material under investigation [52].

6. RESEARCH METHODOLOGY

Water-deteriorated or wet masonry surfaces result in punctual or diffused thermal bridges[19] and consequently in local envelope thermal performance deficiencies and moisture exchange variations.
Since the vapour distribution in materials is not homogeneous, a holistic masonry thermal performance evaluation is necessary, especially if masonry is supposed to experience robust moisten cycles during the year. For better understanding if a masonry presents thermal performance heterogeneities, an iterative IRT throughout different year-periods can be performed and coupled with Heat Flow Metering (HFM) on the evidenced irregular areas.
In historic buildings, where masonry is not homogeneously constructed, the above mentioned consideration is even more significant. In these buildings, indeed, a consistent variation of the thermal performance might be observed through extended areas on the same masonry surface; this might happen due to specific temporary or permanent wall failures; see sect. 3.
This study suggests an indirect methodology for evaluating the masonry thermal performance and its local variations caused by the heterogeneous distribution of moisture. The methodology has been applied in Vleeshuis Museum in Antwerp (Belgium).
In this building, no intrusive diagnosis was allowed, therefore, a specific protocol has been developed based of existing validated onsite diagnostic techniques such as thermal imaging [39], heat flow metering [5] and quasi in contact environmental monitoring [7]. The methodology theoretical background is described in this section, while the monitoring protocol for the investigated case study is presented in section 7. Research results and conclusions are discussed in sections 8 and 9.
Section 6.1 presents the methodology for assessing the masonry thermal homogeneousness: this assessment considers wall surface temperature factor and heterogeneity factor calculation based on Infrared imaging; section 6.2 describes the iterative IRT and moisture exchange monitoring as methodology for localizing moistened areas. Section 6.3 defines the thermal performance evaluation methodology for the studied masonry.

6.1 Masonry surface temperature factor and heterogeneity factor evaluation

Moisture penetrative damp (either from sorption or capillarity) might increase materials' thermal conductivity and evaporative cooling [53]. Therefore, during an IR thermography, the resulting apparent surface temperature of moistened materials, may either be colder (due to the surface evaporation) or warmer (due to the high thermal inertia of water)[20] [22]. It is possible to establish the analogy: *wet material → material thermal bridge*.
Indeed, exactly as in the case of thermal bridges, wet areas reduce wall thermal performance (higher U) and vary the overall *surface temperature factor* (μ_s) and *heterogeneity surface temperature factor* (μ_h) of the masonry, increasing the chances of condensation phenomena, biological infestation and thermophoresis[21].
In this section surface temperature factor and heterogeneity factor, calculated on the basis of iterative IRT results, aim at evaluating the influence of moistened areas on the overall masonry thermal homogeneity.

[19] Punctual thermal bridges as defined in Sect. 3, Terms and definition in EN ISO 10211 [67]
[20] In the latter case, a heat source has to be applied e.g., active infrared thermography.
[21] In order to avoid condensation and thermophoresis phenomena, (μ_h) should be, during the heated period, below 1.5-2; Opaque envelope (in Italian); pp. 198-199 in [58]; Extra (μ_h) compliance values are proposed in Table 6.1.1

The *surface temperature factor* (μ_s) is a non-dimensional parameter commonly used for building elements thermal evaluation purpose. It is defined as the difference between the interior surface temperature and the outdoor air temperature under 1K air temperature difference indoor-outdoor. It is calculated for an arbitrary interior surface point by the formula *(1)* [54][55].

$$\mu_s = \frac{\theta_{si} - \theta_e}{\theta_i - \theta_e} \qquad (1)$$

Where (θ_i) and (θ_e) are the internal and external air dry bulb temperature, while (θ_{si}) is the internal surface temperature on the point; the value decreases if thermal irregularities exist. The minimum value (μ_{sm}), commonly reached in presence of thermal bridges, is calculated by the formula *(2)* in [54].
Minimum (μ_{sm}) threshold values for different Countries climatic conditions are reported by T. Kalameens in [56]; for Belgian climate condition see Table 6.1.1.

$$\mu_{sm} = \frac{\theta_{sm} - \theta_e}{\theta_i - \theta_e} \qquad (2)$$

(θ_{sm}) is the minimum observed wall surface temperature value. If the masonry is interested by moisture deterioration phenomena, the damp areas result in temperature lower than the rest of the surface and this varies locally the wall surface temperature factor. The lower the *surface temperature factor* is, the higher the risk of condensation or biological growth might be. However, in order to evaluate surface condensation in the long term, the dew point temperature (θ_d), has to be evaluated against the surface temperature profile (see section 8). To avoid surface condensation, the internal surface temperature (θ_{si}), has to be above the dew point temperature (θ_d), so the relation in *(3)* has to be always verified.

$$\frac{\theta_d - \theta_e}{\theta_i - \theta_e} < \frac{\theta_{sm} - \theta_e}{\theta_i - \theta_e} \qquad (3)$$

Another method for calculating the *surface temperature factor* (μ_s) is proposed by the formula *(4)* in [54][57].

$$\mu_s^* = \frac{\theta_i - \theta_{si}}{\theta_i - \theta_e} \qquad (4)$$

The *modified surface temperature factor* (μ_s^*) as expressed in *(4)* has to be as low as possible and in any case below 0.25 (see Table 6.1.1).
Beside the surface temperature factor, the *heterogeneity factor* (μ_h), calculated as in formula *(5)*, gives a better understanding on the temperature reduction caused by the moistened areas, in comparison to the rest of the homogeneous surface (not affected by the thermal bridge) with regard to the indoor air temperature. This parameter becomes extremely useful, in the specific case, for evaluating the role played by the moisture in deviating the overall wall surface temperature from the normal values.

$$\mu_h = \frac{\theta_i - \theta_{sm}}{\theta_i - \theta_{si}} \qquad (5)$$

Thresholds for both (μ_s^*) and (μ_h) with the aim of preventing condensation and mold growth, are given in [57][58][55] and reported in Table 6.1.1.

Here Table 6.1.1

6.2 Infrared Thermography (IRT) and hygrothermal monitoring

The indirect investigation, proposed in this study, is based on the environmental monitoring of indoor-outdoor hygrothermal parameters combined with passive infrared thermography and heat flow metering.
IRT together with environmental monitoring of quasi in contact hygrothermal parameters[22] -such as air mixing ratio, air relative humidity, air dew point temperature and air dry bulb temperature- have allowed a good understanding of the dynamic moisture exchange between the wall and the surrounding indoor air mass.
The dryer and wetter areas on the investigated wall surfaces, have been localised and the thermal conductance on these points has been measured and, between them, compared. The thermal performance evaluation of dry and damp wall areas on the same masonry surface has been allowed.
It is worth mentioning that the performed non-intrusive monitoring methodology did not allow to evidence absolute material dryness since no laboratory Equilibrium Material Moisture Content (*EMMC*) measurement was foreseen. Nevertheless, the evaluation and comparison between less moistened areas (lower evaporative moisture exchange) and moistened areas (higher evaporative moisture exchange)[23], together with the iterative IRT, allowed a comprehensive understanding of the relation between localised moisture and specific thermal performance variation.
A methodology, similar to the one here presented, has been implemented by D. Camuffo in prestigious heritage sites [14][26] where no destructive technologies were allowed. The author investigated the air Mixing Ratio (MR) variations for enabling building envelope diagnosis [59]. Physically, the MR (g/kg) represents the ratio between the mass of vapor (m_v) and the mass of dry air (m_a) as expressed by the formula (6) [59].

$$\mathrm{MR}=\frac{m_v}{m_a} \qquad (6)$$

As this ratio is not temperature and pressure dependent, it stays constant unless evaporation or condensation occurs. Therefore, monitoring it over time (quasi in contact with the surface) may allow us to recognise whether the surface is releasing moisture to the environment or absorbing it. A similar indirect moisture damage assessment was proposed by L. Haughton in contemporary buildings [60].
The abovementioned studies were mainly aimed at assessing the overall wall hygrothermal behavior but not at evaluating potential relations between moisture presence and thermal performance variation.

6.3 Thermal performance evaluation

The thermal performance of a building component is generally defined by its thermal transmittance value (*U*) expressed as the integral of the heat flow rate density (q) by the integral of the temperature gradient (inside-outside) over the time, see formula (7).

$$U=\frac{\int q\,dt}{\int(\Theta\mathrm{i}-\Theta\mathrm{e})dt} \qquad (7)$$

During *in-situ* measurements, according to EN 9869 [5], it can be inferred from the measurement of the thermal conductance (Λ), see formula (8).

$$\Lambda=\frac{\sum_{j=1}^{n} qj}{\sum_{j=1}^{n}(\Theta\mathrm{si}j-\Theta\mathrm{se}j)} \qquad (8)$$

[22] *Quasi in contact parameters* are not meant as defined by the EN 15758, but as hygrothermal parameters measured quasi in contact with the wall surface, as recommended by EN 16242; Consideration and recommendations related to measuring methods; pp 9; in [7]
[23] Ensuring indoor air temperature steadiness and avoiding any heat source being in contact with the wall surface of part thereof, such as heating or lighting system.

Where Θsi_j and Θse_j are the measured internal and external surface temperatures at the instant j, and q_j is the measured heat flow rate density at the instant j. By knowing that:
- The thermal resistance (R) is the reciprocal of (Λ) as reported in formula (9)
- The total thermal resistance (R_{tot}) is given by the summation of (R) and the *surface thermal resistances* (R_{si} and R_{se}), as reported in formula (10)
- The thermal transmittance (U) is the reciprocal of (R_{tot}), as reported in formula (11)

$$R = \frac{1}{\Lambda} \tag{9}$$

$$(R_{tot}) = R_{si} + R + R_{se} \tag{10}$$

Where R_{si} and R_{se} are respectively the internal and external surface thermal resistance and R the materials resistance.

$$U = \frac{1}{R_{tot}} \tag{11}$$

the U value can be calculated from formula (12) by considering the internal (h_i) and external (h_e) surface film coefficient for heat transfer [5][61]. The internal and external adduction coefficients have been considered respectively $7.7 W/m^2 K$ and $25 W/m^2 K$.

$$U = \frac{\sum_{j=1}^{n} q_j}{\sum_{j=1}^{n} (\Theta i_j - \Theta e_j)} + h_i + h_e \tag{12}$$

The thermal transmittance value has been calculated according to the moving average method as further discussed in section 7.
The standard uncertainty for the thermal conductance (Λ), therefore, thermal transmittance (U) is calculated as proposed in [62] for each measurement point and reported in Section 8.2.

7. CASE STUDY AND RESEARCH IMPLEMENTATION

The monitored building, the music instruments museum of Antwerp, is a typical medieval Flemish slaughterhouse (Image 7.1). The importance of this outstanding building is not given only by the collection in it contained, but by the building historical significance itself. Although the use destination has changed across the centuries, it is still possible to observe the original architectonic volume.
The building was built ensuring independent uses: the slaughter space, the market space, the residential and storage spaces. These functions were typologically defined by specific architectural features and indoor performance requirements [63]. The slaughter space (Image 7.2) was built in the cellar according to the need of blood and waste disposal; the covered market, where the products were sold, is localised at ground floor (Image 7.3), while spaces for receptions and storage were housed at the upper floors. The study was conducted in one of these latter spaces (Image 7.4). The vertical distribution through the levels is ensured by five towers: one on each building corner and one extra tower on the south façade. Currently the exhibition of musical instruments and paintings related to the musical tradition of the city is at the ground level and in the cellar. The rest of the building is partially used as office and storage.

Here Image 7.1
Here Image 7.2
Here Image 7.3
Here Image 7.4

7.1 Case study constrains

In the whole building, water-related deterioration phenomena are present; however the authors opted for the investigation of a wall at the first floor (although not favorable for its southern orientation) with evident deterioration caused by moisture presence.
On the investigated wall, water infiltration through the component connections together with rainfall and driven rain absorption are the main cause of bricks deterioration and biological infestation on the wall surface. The presence of heating system enables fast moisture evaporation, resulting in salts crystallisation on the internal wall surface.

7.2 *In-situ* monitoring protocol

The monitoring was conducted on the S-W oriented masonry in the first floor of Vleeshuis museum from 07/03/2014 to 07/05/2014. The mean air dry bulb temperature for the whole monitored period was: 21.93°C inside and 12.50°C outside the building. The average air temperature gradient (ΔT) throughout the monitoring period has been 9.43°C.
As unsteady environmental boundary conditions occurred, the thermal transmittance value was calculated by considering the moving average method[24], which consists in calculating the thermal conductance (Λ) by using, for each interval, the averaged values of all the previous intervals, instead of calculating it by averaging the heat flux and temperature difference for the entire monitored period [28]. According to EN 9869 [5], the heat flow meter (HFM) system reaches convergence when the conductance value oscillates around the horizontal asymptote with an amplitude not higher than 0.05 W/m²K from at least 24 hours. In order to obtain this steadiness long monitoring periods were required.
The studied wall is a 100cm tick brick masonry, divided in two sections by windows, with an external continuous course of natural sandstone maximum 23.0 cm deep. As destructive tests were not allowed, the specific wall stratigraphy (although known by literature studies) could not be confirmed by endoscopic inspections, therefore *U* value calculation on the basis of the EN 6946 could not be proposed[25].
After a preliminary visual inspection, IRT of both the wall sections was conducted for detecting moistened areas as well as for identifying a drier area to select as benchmark for the successive comparative analyses. For better interpreting surface moisture dynamic variations, the wall sections have been gridded in regular 50*50cm elements and iterative IR assessment was performed on a 2-week basis. The measurement points on which hygrothermal parameters and thermal conductance were measured have been identified according to the grids: A3, H3, H7, I5, I7 (See Image 7.2.1 and 7.2.2).
The window shutters, during the whole monitoring period, were kept closed to avoid direct solar radiation, moreover the radiators were switched off for not interfering with the experimental measurements.

Here Image 7.2.1
Here Image 7.2.2

The main goal of the iterative assessment was to evaluate potential abrupt moisture paths variations and to promote a cross-check between IRT outcomes and hygrothermal monitoring results (see section 8.1 and 8.2).
Furthermore, on the basis of iterative IRT, the masonry's *surface temperature factor* (μs) and *heterogeneity temperature factor* (μh) were calculated for evaluating wherever risks of condensation or biological growth occurred and to assess the extent of thermal heterogeneity due to the heterogeneous moisture distribution (see section 8).
Surface temperatures and heat flows were measured with heat flow meter (HFM) on the benchmark point (driest area) and on comparative points per each wall section (wet areas). Thus wall thermal conductance (*Λ*) was measured and thermal transmittance (*U*) was calculated. The obtained results were, hence, compared.

24 Also known as Progressive average method
25 As the EN 6946 proposes *U* value calculation methodology based on perfectly known stratigraphy, it should be avoided whenever there is no certainty on the material thicknesses.

Next to surface temperature and heat flow, the moisture masonry exchange, quantified by the air mixing ratio (MR), as well as air dry bulb temperature (T), dew point temperature (Tdw) and relative humidity (RH) were measured, with 10min time interval, at 5mm distance from the wall surface, in each selected measurement point as recommended by the EN 16242 [7].
The monitoring activities are summarised in Table 7.2.1 and a graphical monitoring flow chart is proposed in Image 7.2.3. The instruments accuracy and specifications are reported in Table 7.2.2 (Hobo U 10 Data Logger), Table 7.2.3 (FLIR E60BX Infrared Camera), Table 7.2.4 (ThermoZig Heat Flow Meter).

Here Table 7.2.1
Here Table 7.2 2
Here Table 7.2 3
Here Table 7.2 4
Here Image 7.2.3

8. EXPERIMENTAL RESULTS DISCUSSION

The results discussion in this section is divided in IRT-assessment and Hygrothermal-assessment. This distinction, based on the monitoring activities, allows an independent result appraisal; jointed conclusions are successively discussed in section 9.

8.1 IRT masonry assessment

During the first IRT, the surface temperature heterogeneity on the two wall sections was evaluated and moistened areas were identified.
In the first wall section (Images 8.1.1-8.1.4), an extended damp area was visible on the central part of the surface, namely on the connection ceiling- parietal wall. This area, triangular-shaped, extends until the lower right corner on the wall section passing behind the painting on the wall. During the monitoring campaign, the canvas could not be removed from its position, so it was not possible to evaluate the moisture path behind it.
On the upper part of this first masonry section, the surface average temperature difference between moist and dry area was 2.1°C (see Image 8.1.1). However, punctual temperature differences up to 3.8°C were observed in less than 2m distance between two wall spots (See Image 8.1.1).
Although moisture presence has been found more concentrated in the central wall section part, causing the characteristic robust increase of evaporative cooling and temperature reduction, it was not possible to position heat flow measurement points on this area (as not reachable from outside), therefore another representative measurement point on the edge of the moistened area (towards the right section corner) has been measured (H7).
Point H7 is localised on an area in which, although with less intensity than the central part, moisture presence was clearly observed, see Image 8.1.3. As the point is on a corner area, the typical effects produced by the solar radiation, such as speeding of evaporating exchange and surface temperature variation, were limited by the positioning of the sensors 50cm far from the corner, furthermore, window shutters were kept closed to decrease the influence of direct solar gains.
On the bottom part of the same section, the damp area is only localised on the right corner. On this area, H3 point has been measured. As it is possible to see in Image 8.1.4, the average surface temperature in the damp area (on the right) is 1.2°C different from the non-damp area (on the left). The entire left side of the first wall section from the bottom (Image 8.1.4) to the top (Image 8.1.1) is characterised by unchanged surface temperature. The temperature field was apparently not influenced by moisture dynamics, so this area was considered as a benchmark for the successive comparisons.
In-contact surface temperatures and heat flows together with -quasi in contact- air hygrothermal parameters, were monitored on the above mentioned points. Table 8.1.1 reports the set of measured quantities for each measurement point, for both the masonry sections.

Here Image 8.1.1, 8.1.2, 8.1.3, 8.1.4

Here Table 8.1.1

The second wall section showed moisture concentration on the central area as it was found in the first wall section. However the extension of the moist surface on section II is more diffused than the one found in section I. The edges of the wet area are less sharp than the ones observed in section I, evidencing a slower evaporative moisture exchange.
The observed temperature gradient between moist and dry areas is smaller than the previous wall section. The maximum observed average surface temperature difference was 1°C, however spot temperatures reach 2.2°C variation between dry and damp areas (Images 8.1.5 and 8.1.6).
Also in this case the right side of the masonry section showed a heterogeneous temperature distribution given by the moisture variation; this was observed from the top (Image 8.1.7) to the bottom (Image 8.1.8). Conversely, a more homogeneous temperature field was observed on the left wall side.
Also in this case the painting on the wall could not be removed, therefore no information on the moisture presence and its distribution behind it can be delivered.
In section II two points on the damp area, namely I5 and I7, have been measured and their results were compared to the benchmark (A3). However, since point I5 was temporary influenced by solar gains, according to the followed methodology it was eliminated from the study and not further discussed (see Image 7.2.3).

Here Image 8.1.5
Here Image 8.1.6
Here Image 8.1.7
Here Image 8.1.8

8.2 Hygrothermal masonry evaluation

Surface temperature factors and heterogeneity factors, for both the wall sections, have been iteratively calculated based on the iterative IRT. Two representative moments of the monitoring are plotted and discussed: March the 7th and April the 14th, respectively at the beginning and at a late stage of the monitoring campaign.
In Graph 8.2.1, the surface temperature factor distribution (μ_s^*) is plotted with regard to wall section I on March the 7th.

Here Graph 8.2.1
Here Table 8.2.1

On the wall section, the (μ_s^*) average resulted 56% higher than the suggested threshold (See Table 6.1.1). The strongest deviations occurred on the areas evidenced as damp, especially on the central upper part (See Section 8.1).
On this wall section, due to the surface temperature reduction caused by the robust moisture presence, (μ_s^*) values increased up to 0.67, far higher from the suggested 0.25 maximum limit [54][57]. These extreme conditions may predispose the wall to masonry surface condensation, biological growth or materials deterioration. Beside the (modified) surface temperature factor, the relation in *(3)* had to be verified for evaluating the surface condensation risk throughout the whole monitored period.
As expected the surface temperature factor decreases towards the left side of the section since the wall was drier. On this part, where the wall benchmark has been selected (See A3 in 7.2.1 and 8.2.1), the (μ_s^*) average was 0.19, perfectly in compliance with the recommended value.
On the central bottom area (Graph 8.2.1), the (μ_s^*) value slightly rose; it decreased again on the lower corner side (where point H3 was selected), and it rose once again towards the upper right part (where point H7 was selected). Clearly the *surface temperature modified factor* (μ_s^*) increased accordingly to the moisture patterns, reaching high critical levels on the central wall area, where the strongest moisture problems were registered.

In table 8.2.1, a data summary for wall section I on March the 7th is presented. On this wall section the calculated mean temperature factor was 0.61 and the minimum reached value was 0.33 (see Graph 8.2.1). Therefore surface temperature factor (μ_s) has been registered always below the suggested minimum required value [55].
The calculated heterogeneity factor (μ_h) for the wall section I was 1.73, in compliance with the maximum threshold value (Table 6.1.1).
During the same monitoring day, on wall section II, again strong deviations between recommended and calculated surface temperature factor values were found (see Graph 8.2.2). The average *modified surface temperature factor* (μ_s^*) was 0.44 and it rose up to 0.61 on the moistened areas(μ_s^*). This happened on the lower and upper right side and on the upper central part of the wall (See Graph 8.2.2). The average (μ_s), in the second wall section, was 0.56, but the minimum reached value was 0.39, extremely lower than the suggested 0.70 [55].
The heterogeneity factor was 1.39 (See Table 8.2.2), lower than the one registered in section I, but again perfectly in compliance with the recommended interval (See Table 6.1.2). However, it has to be pointed out that the heterogeneity factor on its own does not give the whole image of a potential problem, as it has to be evaluated together with the other mentioned factors. The calculated factors summary, for walls section II on March the 7th, is given in Table 8.2.2.

Here Graph 8.2.2
Here Table 8.2.2

On the 14th of April, both the surface temperatures and the heterogeneity factors on the wall sections showed the same trend and distribution already observed during the 7th of March. Nevertheless the difference between calculated and recommended values has been found smaller than the ones calculated with regard to the previous monitored period; this enabled a general fulfillment of the calculated parameters to the recommended thresholds.
In Graph 8.2.3, the (μ_s^*) distribution in wall section I is shown. It is evident how the values reproduce exactly the same pattern obtained on March 7th; however the values are drastically reduced by half. This situation likely occurs because of the natural material drying.
The central upper part of the wall surface was still the one with higher values; but since the maximum value was ≤ 0.25, the wall can be considered in compliance with the thresholds proposed in Table 6.1.1. The average surface temperature factor was 0.90 and its minimum value 0.76, higher than 0.70 as suggested in Table 6.1.1.

Here Graph 8.2.3
Here Table 8.2.3
Here Graph 8.2.4
Here Table 8.2.4

Similarly, the situation was improved also in section II (see Graph 8.2.4), where the previous maximum (μ_s^*) value decreased by 68.8%, and the current maximum value is 0.25. Also the *minimum surface temperature factor* (μ_{sm}) previously equal to 0.39, on April 14th, rises until the safeguard value of 0.76. The (μ_s) average was 0.87, increased by 55% compared to the one calculated in March. The interior surface temperature increase produced a general stabilisation of the values out from the risky ranges.
The warming of the interior wall surface has produced a general reduction of the difference between mean surface wall temperature (θ_{si}) and minimum surface wall temperature (θ_{sm}) and a strong reduction on the difference between indoor air temperature (θ_i) and mean surface wall temperature(θ_i). However, the heterogeneity factor (μ_h), expression of the coldest point deviation from the surface mean temperature on the basis of the indoor air temperature (see Formula 5), increased for both the wall sections (see data summary on Table 8.2.3 and Table 8.2.4).
This condition occurs because the variation between indoor air temperature and minimum surface temperature in both the wall sections decreased less than the variation between -indoor air temperature and

mean wall temperature if comparing the configuration in March to the one in April; indeed, the difference $(\theta_i - \theta_{si})$ is reduced by 60% in wall section I and 50% in wall section II and the difference $(\theta_i - \theta_{sm})$ is reduced by 39% and 30% in wall section I and II respectively. This produced, in accordance with formula (5), a substantial increase of the heterogeneity factor (μ_h).
By considering the fact that minimum surface temperature values are still observed in the previously assessed damp areas, it is possible to conclude that the residual moisture presence in the damp masonry areas, did not allow a surface temperature increase proportional to the rest of the wall surface.
Therefore, although an absolute surface temperature increase also on the colder areas exists, its temperature rise compared to the rest of the homogeneous wall was too low and the heterogeneity factor was not reduced. This phenomenon might be reasonably explained by the increased thermal capacity of the moist masonry bricks as described in section 3.

Here Table 8.2.5

In order to draw conclusion on the potential risk of surface condensation on the investigated wall sections, the relation in (*3*) has to be verified for both the discussed periods. The results from the calculation are reported in Table 8.2.6.

Here Table 8.2.6

N.B, the first term in *(3)* expresses the surface temperature factor at the dew point temperature (μ_d), while the second term, already discussed (see Section 6.1), expresses the minimum surface temperature factor (μ_{sm}).
As showed in Table 8.2.6, the first term is always lower than the second one in both the sections for both the periods verifying the relation in (3). No surface condensation during the observed two moments in March and April occurred.
It is worth mentioning that the above discussed surface condensation verification, is not representative for the whole monitoring period. In order to allow a verification throughout the whole monitoring period, the air dew point temperature (T_{dew})in the room and the quasi-in contact surface dew point temperature (T_{qdew}) for the selected points [26] have been plotted and evaluated against the point surface temperature (T_{si}).
As it is clear from the graphs (8.2.5 to 8.2.8), wall surface temperature has been always higher than the dew point temperature during the March –May monitored period, therefore no surface condensation occurred.

Here Graph 8.2.5
Here Graph 8.2.6
Here Graph 8.2.7
Here Graph 8.2.8

The dynamic trends of Mixing Ratio (MR) with regard to: benchmark point (A3), selected points onto the moistened wall surface areas (H3, H7, I7) and room itself are discussed below.
Since MR analysis is susceptible to misunderstanding, caution should be paid when measuring it over the space; unwanted thermal solicitations should be avoided. For this reason it was decided, as already reported, not to consider results from point I5, as it was not possible to completely avoid the solar radiation.
In Graph 8.2.9, air MR hourly variations at 5mm distance from the selected points on the investigated masonry against the air MR in the middle of the room (four meter distance from the investigated masonry) are plotted.

Here Graph 8.2.9

[26] As proposed in 5.1 Consideration and recommendation related to measuring method; pp 9-10; in EN 16242 [7]

By considering the findings from the IRT (see section 8.1) and the results from the surface temperature and heterogeneity factor analysis, it is evident that masonry moisture, for the whole monitoring period, constantly evaporated into the heated space and never condensed on the wall surface.
The highest moisture exchange and consequently the highest evaporative cooling, was observed close to the wetter areas: respectively in H7 and I7, the mean MR has been respectively 11.32 g/kg and 11.16 g/kg (Graph 8.2.9). It has to be pointed out that, although the evaporative exchange during the typical day was slightly influenced by the background building heating schedule, the quasi in contact air temperature layering (due to convective exchanges) was avoided by keeping the radiators constantly switched off for the whole monitored period.
During the iterative IRT, Point H3 resulted colder than the benchmark (A3) but warmer than I7 and H7; in this point, the quasi in contact mean MR was 9.25 g/Kg (see section 8.1), while on the benchmark point (A3), remarkably drier than the other studied points, the mean MR was 8.60g/Kg. However, the lowest MR value was logically observed in the center of the room; for the whole monitoring period it has been 7.57 g/Kg.

Here Graph 8.2.9

The thermal masonry performance has been evaluated by measuring the thermal conductance (Λ) for each of the mentioned points (A3, H3, H7 and I7).
The consequent thermal transmittance (U), on the basis of the heat flow metering results, has been calculated by both mathematical average and movable average method.
In Graph 8.2.10 it is evident the increase of thermal transmittance value on the points evidenced with stronger moisture exchange.

Here Graph 8.2.10

Point A3 (baseline) either during IR thermography or evaporative cooling analysis and surface temperature factor analysis, has been evidenced as the driest area of the wall. On this point the lowest thermal transmittance value (0.478 W/m²K) was recorded.
The U value gradually rose on the areas evidenced as the most influenced by moisture presence: in point H3, H7 and I7, the thermal transmittance was found respectively 69%, 70% and 71% higher than the baseline point (A3). Although eventual presence of cracks or geometrical irregularities might exist, the results confirmed the unavoidable influence of moisture on the thermal properties variation of hygroscopic components such as traditional brick masonries.
In Table 8.2.7 the deviation between the U value moving average and the U value mathematical average per each measured point is reported. The highest variation has been evidenced in point H7 where the difference between the two calculation methodologies is almost 22%. With regard to the rest of the points, the deviation between the methods is always lower than 15%.
According to EN 9869 [5] the average method is not recommended for monitoring campaigns not performed in steady conditions. Therefore the results obtained from the moving average method should be preferred.

Here Table 8.2.7

The experimental standard deviation for the measured independent variables[27] (internal and external surface temperature and heat flow) as well as the thermal conductance combined standard uncertainty, calculated as the positive root square of the combined variance of each measured independents variable[28] are both plotted in Table 8.2.8.
The maximum thermal conductance uncertainty is soundly observed where the experimental external surface temperature standard deviation is higher (see measurement points H3 and H7). This condition

[27] Calculated as in Sect. 4.2 Type A evaluation of standard uncertainty; 4.2.2 experimental variance of the observations; p. 10; [62]
[28] Calculated as in Sect. 5 Determining combined standard uncertainties; 5.1 Uncorrelated input quantities; pp. 18-19 in [62]

caused the temperature gradient reduction, resulting in a slight increase of the heat flow standard deviation and a less accurate thermal conductance-transmittance.

Here Table 8.2.8

9. CONCLUSIONS

In this study an indirect monitoring methodology aimed at evaluating the masonry thermal performance and its variation according to moisture distribution has been proposed. The monitoring was carried out, by means of non-invasive or destructive diagnosis, in Vleeshuis Museum in Antwerp (Belgium) from March to May 2014.

Wall thermal inhomogeneities, caused by moisture distribution, were investigated in order to assess the thermal transmittance value deviation between masonry dry and moistened areas of a traditional brick wall. Quasi in contact hygrothermal monitoring together with iterative Infrared imaging and heat flow monitoring allowed to outline that, although the investigated masonry is subjected to natural drying, it does not dry homogeneously. This phenomenon, mainly caused by the heterogeneous moisture distribution, is shown by the increase of the surface temperature heterogeneity factors.

A progressive reduction of the difference between mean indoor air temperature and mean masonry surface temperature, confirmed masonry homogenization and drying by the end of the monitoring period. However, the damp areas, although progressively warmer and drier, showed punctual surface temperature far colder than the rest of the masonry; this is explained by the presence of residual moisture on the specific areas. Also confirmed by Infrared imaging.

The increase of the surface heterogeneity factor was caused by the low closeness between masonry surface mean temperature and minimum surface temperature.

An evident partialization of the masonry thermal performance, consisting in a thermal transmittance increase up to 3 times on the wet areas compared to the driest one, was registered. The moistened points revealed thermal transmittance value from 69% (H3) to 71% (I7) higher than the driest masonry surface (A3). These findings confirm the driving role played by the moisture in radically perturbing the thermal properties of building components.

Local moisture presence might causes, as in the presented case study, simultaneous increase of thermal transmittance value, evaporative cooling and masonry surface heterogeneity factor, generating thus an irregularly distributed thermal bridge.

According to the described findings, moisture incidence should be onsite evaluated before any envelope retrofitting strategy or intervention proposal as its influence can nullify the effectiveness of any insulation proposition.

This consideration in historic buildings becomes even more stringent as aging phenomena can strongly affect the hygrothermal behavior of envelope components leading to localized loss of performance. Eventual failures conditions should be *in-situ* evaluated previously to any retrofitting proposition. If, because of building preservation requirements, no invasive preliminary diagnosis are allowed, indirect assessment methodologies, such as the one presented in this contribution, should be ad hoc developed.

10. ACKNOWLEDGMENTS

The authors would like to acknowledge arch. Hans Goossens, ir. Geoff Coninx, ir. William Vercauteren and the whole staff of Vleeshuis Museum for their kind support during this research.

11. REFERENCES

[1] European Union, Directive 2002/91/EC of the European Parliament and of European Council of 16 December 2002 on the energy performance of buildings. 2003, pp. 65–71.

[2] European Union, Directive 2010/31/EU of the European Parliament and of the Cauncil of Europe of 19 May 2010 on the energy performance of buildings (recast). 2010, pp. 13–35.

[3] BPIE: Building Performance Institute of Europe, Europe ’ s buildings under the microscope. 2011.

[4] P. a. Fokaides and S. a. Kalogirou, “Application of infrared thermography for the determination of the overall heat transfer coefficient (U-Value) in building envelopes,” Appl. Energy, vol. 88, no. 12, pp. 4358–4365, Dec. 2011.
[5] CEN European Commitee for Standardization, EN 9869-Thermal Insulation-building elements- In situ measurements of thermal resistance and thermal transmittance, vol. 1994. 1994.
[6] C. of Europe, “Second European Conference of Ministers responsible for the Architectural Heritage,” Granada, 1985.
[7] N. CEN, “NBN EN 16242 Conservation of cultural heritage- Procedure and instruments for measuring humidity in the air and moisture exchanges between air and cultural property,” 2013.
[8] NBN EN ISO, EN ISO 6946 Building components and building elements -Thermal resistance and Thermal transmittance- Calculation method (ISO 6946:2007). 2008.
[9] R. Adhikari, E. Lucchi, and V. Pracchi, “Experimental measurements on thermal transmittance of the opaque vertical walls in the historical buildings,” in PLEA2012 Conference, Opportunities, Limits and Needs Towards an environmentally responsible architecture, 2012.
[10] G. Litti, A. Audenaert, and J. Braet, “Energy Retrofitting in Architectural Heritage, Possible Risks Due to the Missing of a Specific Legislative and Methodological Protocol,” in The European Conference on Sustainability , Energy and the Environment 2013 Official Conference Proceedings, 2013.
[11] R. Hendrickx, H. De Clercq, F. Decock, and F. Descamps, “Hygrothermal analysis of the façades of the former veterinary school in Anderlecht (Belgium) for the risk assessment of internal thermal insulation,” pp. 1092–1098, 2013.
[12] C. Herman, “High and Low impact strategies for the internal insulations retrofit of traditional masonry walls,” in 3 rd European Workshop on Cultural Heritage Preservation, EWCHP 2013, 2013, pp. 181–188.
[13] W. C. Brown, C. J. Shirtliffe, and A. H. P. Maurenbrecher, “Monitoring of the building envelope of a heritage house : a case study,” no. March 1993, 1999.
[14] D. Camuffo, “Indoor dynamic climatology: investigations on the interactions between walls and indoor environment,” Atmos. Environ., vol. 17, no. 9, pp. 1803–1809, 1983.
[15] D. Camuffo, A. della Valle, C. Bertolin, C. Leorato, and A. Bistrot, “Humidity and environmental diagnostics in Palazzo Grimani, Venice,” in Indoor environment and preservation, climate control in museums and historic buildings, D. del Curto, Ed. Kermes, 2011, pp. 45–50.
[16] A. Antonyová, A. Korjenic, P. Antony, S. Korjenic, E. Pavlušová, M. Pavluš, and T. Bednar, “Hygrothermal properties of building envelopes: Reliability of the effectiveness of energy saving,” Energy Build., vol. 57, pp. 187–192, Feb. 2013.
[17] S. Doran, “DETR Framework Project Report; Safety and Health Business Plan Field investigations of the thermal performance of construction elements as built,” Glasgow, 2001.
[18] P. Baker, G. Caledonian, and H. Scotland, “U values and traditional buildings,” Glasgow, 2011.
[19] F. Asdrubali, G. Baldinelli, and F. Bianchi, “A quantitative methodology to evaluate thermal bridges in buildings,” Appl. Energy, vol. 97, pp. 365–373, Sep. 2012.
[20] R. Albatici and A. M. Tonelli, “Infrared thermovision technique for the assessment of thermal transmittance value of opaque building elements on site,” Energy Build., vol. 42, no. 11, pp. 2177–2183, Nov. 2010.
[21] P. G. Cesarotto and M. De Carli, “A measuring campaign of thermal conductance in situ and possible impacts on net energy demand in buildings,” Energy Build., vol. 59, pp. 29–36, 2013.
[22] E. Rosina and N. Ludwig, “Optimal thermographic procedures for moisture analysis in building materials.” Milan, 2010.
[23] D. A. Haralambopoulos and G. S. Paparsenon, “Assessing the thermal insulation of old buildings- the need for in situ spot measurements of thermal resistance and planar infrared thermography,” vol. 39, no. 1, pp. 65–79, 1998.
[24] N. M. M. Ramos, J. M. P. Q. Delgado, E. Barreira, and V. P. De Freitas, “Hygrothermal Numerical Simulation : Application in Moisture Damage Prevention,” 2007.

[25] C. Ferreira, DeFreitas, V. P, and N. M. . Ramons, “Quantifying the influence of hygroscopic materials in the fluctuations of relative humidity in museums housed in old buildings,” in NSB 10th Nordic Symposium on Building Physics, 2014, pp. 600–607.

[26] D. Camuffo, A. Della Valle, C. Bertolin, C. Leorato, and C. Bristot, “Humidity and Environmental diagnostics in Palazzo Grimani, Venice,” in Indoor environment and preservation, climate control in museums and historic buildings, Nardini, Ed. Florence, 2010, pp. 45–50.

[27] G. Accardo and D. Camuffo, “Microclimate inside the Scrovegni Chapel in Padua,” in Conservation within historic buildings: preprints of the contributions to the Vienna congress, 7-13 September 1980, 1980, pp. 15–17.

[28] S. R. Duverne and P. Baker, “Research into the thermal performance of traditional brick walls,” English Herit. Rep., 2013.

[29] M. Pavlíková and D. Ph, “Hygric and thermal properties of materials used in historical masonry,” 2002.

[30] D. Browne, “The SPAB Hygrothermal Modelling : Interim Report,” no. October, 2012.

[31] F. Ochs, W. Heidemman, and M.-S. H., “Effective Thermal conductivity of the insulation of high temperature underground thermal stores during operation,” in Ecostock 2006, 2006, pp. 1–7.

[32] M. Jerman and R. Černý, “Effect of moisture content on heat and moisture transport and storage properties of thermal insulation materials,” Energy Build., vol. 53, pp. 39–46, Oct. 2012.

[33] 3 encult; efficient energy for EU cultural Heritage, “D7.7 Relation historic buildings, EPBD and EPBD CEN Standards,” 2011.

[34] R. S. Adhikari, E. Lucchi, and V. Pracchi, “Experimental Measurements on Thermal Transmittance of the Opaque Vertical Walls in the Historical Buildings,” no. November, 2012.

[35] P. Biddulph, V. Gori, C. a. Elwell, C. Scott, C. Rye, R. Lowe, and T. Oreszczyn, “Inferring the thermal resistance and effective thermal mass of a wall using frequent temperature and heat flux measurements,” Energy Build., vol. 78, pp. 10–16, Aug. 2014.

[36] E. Genova and G. Fatta, “Contributo alla conoscenza delle proprietà termofisiche delle murature palermitane,” in 30th International Conference on Science and Cultural Heritage, 2014, pp. 809–819.

[37] S. Doran and B. Carr, “Thermal transmittance of walls of dwellings before and after application of cavity wall insulation; Report number 222077,” Glasgow, 2008.

[38] CEN European Commitee for Standardization, “EN 6946:1999 - 30-09-1999 - Componenti e elementi per edilizia - Resistenza termica e trasmittanza termica - Metodo di calcolo.,” 2005.

[39] CEN European Commitee for Standardization, NBN EN 13187 Thermal Performance of Buildings - Qualitative detection of thermal irregularities in building envelopes-Infrared method (ISO 6781:1983 modified). 1999, pp. 1–21.

[40] C. a. Balaras and a. a. Argiriou, “Infrared thermography for building diagnostics,” Energy Build., vol. 34, no. 2, pp. 171–183, Feb. 2002.

[41] A. Kylili, P. a. Fokaides, P. Christou, and S. a. Kalogirou, “Infrared thermography (IRT) applications for building diagnostics: A review,” Appl. Energy, vol. 134, pp. 531–549, Dec. 2014.

[42] R. P. L. E. Ş. U, G. Teodoriu, and G. Ţ. Ă. Ranu, “INFRARED THERMOGRAPHY APPLICATIONS FOR BUILDING INVESTIGATION,” no. Lxii, 2012.

[43] E. Grinzato, N. Ludwig, G. Cadelano, M. Bertucci, M. Gargano, and P. Bison, “Infrared Thermography for Moisture Detection : A Laboratory Study and In-situ Test,” no. January, pp. 97–104, 2011.

[44] L. Capineri, D. Capitani, U. Casellato, P. Faroldi, E. Grinzato, N. Ludwig, R. Olmi, S. Priori, N. Proietti, R. Ruggeri, A. Sansonetti, L. Soroldoni, and M. Valentini, “Limits and Advantages of Different Techniques for Testing Moisture Content in Masonry,” no. January, pp. 111–116, 2011.

[45] E. Rosina, N. Ludwig, and L. Rosi, “Optimal environmental conditions to detect moisture in ancient buildings: case studies in Northern Italy,” in PROCEEDINGS OF THE SOCIETY OF PHOTO-OPTICAL INSTRUMENTATION ENGINEERS (SPIE), 1998, pp. 188–199.

[46] M. C. Phillipson, P. H. Baker, M. Davies, Z. Ye, a. McNaughtan, G. H. Galbraith, and R. C. McLean, “Moisture measurement in building materials: an overview of current methods and new approaches,” Build. Serv. Eng. Res. Technol., vol. 28, no. 4, pp. 303–316, Nov. 2007.

[47] R. Olmi, S. Priori, D. Capitani, N. Proietti, L. Capineri, P. Falorni, R. Negrotti, and C. Riminesi, “Innovative Techniques for Sub-surface Investigations,” 2011, no. January, pp. 89–96.
[48] S. I. Ivashov, V. V Razevig, I. A. Vasiliev, A. V Zhuravlev, T. D. Bechtel, M. College, and L. Capineri, “Development and Applications of the Holographic Subsurface RASCAN Radar,” pp. 1–24, 2010.
[49] L. Capineri, P. Falorni, S. Ivashov, A. Zhuravlev, I. Vasiliev, V. Razevig, T. Bechtel, and G. Stankiewicz, “Combined Holographic Subsurface Radar and Infrared Thermography for Diagnosis of the Conditions of Historical Structures and Artworks,” in EGU General Assembly 2009, 2009, p. 5343.
[50] L. Calegari, D. A. Gatto, and D. M. Stangerlin, INFLUENCE OF MOISTURE CONTENT , SPECIFIC GRAVITY AND SPECIMEN GEOMETRY ON THE ULTRASONIC PULSE VELOCITY IN Eucalyptus grandis Hill ex Maiden WOOD, no. 2177–6830. Ciência da Madeira (Braz. J. Wood Sci.), Pelotas, 2011.
[51] R. Y. VUN, C. B. Mahesh, K. HOOVER, J. JANOWIAK, J. KIMMEL, and S. WORLEY, “Development of Non-contact Ultrasound as a Sensor for Wood Moisture Content,” pp. 1–7, 2006.
[52] D. Camuffo and C. Bertolin, “TOWARDS STANDARDISATION OF MOISTURE CONTENT MEASUREMENT IN CULTURAL HERITAGE MATERIALS,” pp. 23–35, 2012.
[53] M. Fox, D. Coley, S. Goodhew, and P. de Wilde, “Thermography methodologies for detecting energy related building defects,” Renew. Sustain. Energy Rev., vol. 40, pp. 296–310, Dec. 2014.
[54] J. G. M. Alface Pereira Valerio, “Impact Assessment of Thermal Bridges on Residential Buildings Performance,” 2007.
[55] W. En, T. Centrum, and V. Het, “Vochthuishouding in gebouwen; Schadeoorzaken, koude bruggen, binnenklimaat; Gegevens voor ontwerp en uitvoering van gebouwen Woonvoorwaarden van gebouwen,” Brussels, 1984.
[56] T. Kalamees, “Critical values for the temperature factor to assess thermal bridges,” pp. 218–229, 2006.
[57] Y. Couasnet, Les condensations dans les batiments, Presses de. Paris, 1990.
[58] E. Lucchi, Diagnosi energetica strumentale degli edifici. Termografia e analisi non distruttive. Normativa e procedure operative. Palermo (Italy), 2012.
[59] D. Camuffo, “Microclimate for Cultural Heritage.” Elsevier Science, Amsterdam, the Netherlands, pp. 298–314, 1998.
[60] L. Haughton, “Using Humidity/Temperature loggers for moisture investigations: case studies,” in Symposium on building envelope technology , October, 2009, pp. 43–54.
[61] H. Hens, Building Physic- Heat, Air and Moisture; Fundamentals and Engineering methods with examples and exercises, Wilhelm Er. Berlin: Wilhelm Ernst & Sohn, 2012.
[62] J. C. for G. in M. (JCGM/WG1), Evaluation of measurement data — Guide to the expression of uncertainty in measurement, no. September. 2008.
[63] J. Van Herk, “Het Vleeschhuis te Antwerpen,” Jaarboek van Antwerpen’s Oudheidkundige kring, Antwerpen, 1939.
[64] FLIR, “FLIR Users’s manual, Flir Exx series.” .
[65] a. Abdou and I. Budaiwi, “The variation of thermal conductivity of fibrous insulation materials under different levels of moisture content,” Constr. Build. Mater., vol. 43, pp. 533–544, Jun. 2013.
[66] CEN European Commitee for Standardization, EN 1745 Masorny and masonry products; Methods for determining design thermal values. 2005.
[67] CEN European Commitee for Standardization, NBN EN ISO 10211Thermal bridges in building construction- Heat flows and surface temperatures-Detailed calculations. 2008.

Method	**Infrared thermography**	**Nuclear magnetic resonance (NMR)**	**Radar**	**Ultrasound**
Investigation depth	Surface	Up to 20 mm	Up to 200mm	In depth
Type	Qualitative	Quantitative	Qualitative	Qualitative
Constrains	Sensitive to environmental condition	Presence of Iron, polymer-based or organic materials	it is only applicable on flat surfaces	Sensitive to discontinuities or inhomogeneities

Table 5.1; currently implemented Non Destructive Techniques aimed at material moisture detection

Parameter (x)	Value	Reference
(μ_s^*)	x <0.25	[57]
(μ_h)	x < 2	[57]
	x<1.5-2	[58]
(μ_{sm})	x>0.75	[55]

Table 6.1.1; Optimal values for: surface temperature modified factor (μ_s^*)*, minimum surface temperature factor* (μ_{sm}) *and heterogeneity surface temperature factor* (μ_h) *during heated periods* [57][58][55]

Image 7.1; Vleeshuis museum in Antwerp

Image 7.2; Vleeshuis museum, basement level; former slaughter space and actual exhibition space

Image 7.3; Vleeshuis museum, ground level; former market space and actual exhibition space

Image 7.4; Vleeshuis museum, first level; former domestic space and actual storage and multifunctional space

Activity	Aim	Instrument/ Standard	Period
Preliminary Inspection and first IRT	- Evaluation of the wall surface temperature heterogeneity and identification of damp and dry areas - Selection of the measurement points	IR camera (EN 13187)	February 2014
Wall surface gridding and iterative IRT	- Evaluation of thermal surface variation- Identification of average surface temperature for successive calculation of surface temperature factor and heterogeneity surface temperature factor	IR camera, tape and cord (EN 13187)	07/03/2014 - 07/05/2014
Surface temperature and Heat flow measurement (HFM)	- Monitoring surface temperature and heat flow for successive thermal conductance and thermal transmittance calculation	HFM (EN 9869)	07/03/2014- 07/05/2014
Quasi in contact hygrothermal measurement on the masonry and indoor-outdoor hygrothermal measurement	- Monitoring of dry air temperature, relative humidity, mixing ratio, dew point temperature	HOBO Loggers (EN 16242)	07/03/2014- 07/05/2014

Table 7.2.1; Summary of monitoring activities

Measurement range Temperature	-20° to 70°
Measurement range Relative Humidity	25% to 95%
Accuracy Temperature	± 0,4° from 0° to 40° C
Accuracy Relative Humidity	± 3,5% from 25% to 85% over the range of 15° to 45°; ±5 from 25% to 95% over the range of 5° to 55°C
Drift Temperature	0,1°C/year
Drift Relative Humidity	< 1% per year
Response time in airflow of 1m/s Temperature	10 minutes, typical to 90%
Response time in airflow of 1m/s Relative Humidity	6minutes, typical to 90%
Time accuracy	Approximately ±1 minute per month at 25°
Operating range	Logging -20° to 70° Temperature; 0 % to 95% RH

Table 7.2 2; Hobo U 10 Temperature/Relative Humidity Data logger

Temperature resolution:	0.15 °C
Minimum distance measurement:	0.6m
Working temperature:	-20...+250°C
Error of temperature measurement:	±2 °C, ±2% of the measured value
Emission factor:	0.1...1.0
Indication:	2.8" LCD
Field of View:	12.5° x 12.5°
Full radiometric data:	+
Measurement mode:	Standard measurement (1 point)
image Storage:	Standard JPEG
Storage Capacity:	Mini SD card 512 MB (about 5,000 images)
Software:	Flir tools
Weight:	365g
Dimensions L x W x H:	223 x 83 x 79mm

Table 7.2.3; FLIR E60BX Infrared camera

Temperature Sensor	
Response time (seconds)	8
operative range (°C)	-50...125
Resolution (°C)	0.01
Accuracy (°C)	±0.1
Heat Flow Sensor	
Response time (minutes)	4
operative range (W/m²)	-300...300
Resolution (W/m²)	0.01
Accuracy (%/Temp°C)	±5 (Temp 20°C)
Temperature Range (°C)	-20...60
Thermal Resistance (m²K/W)	<0.006

Table 7.2.4; ThermoZig Light Heat Flow Meter

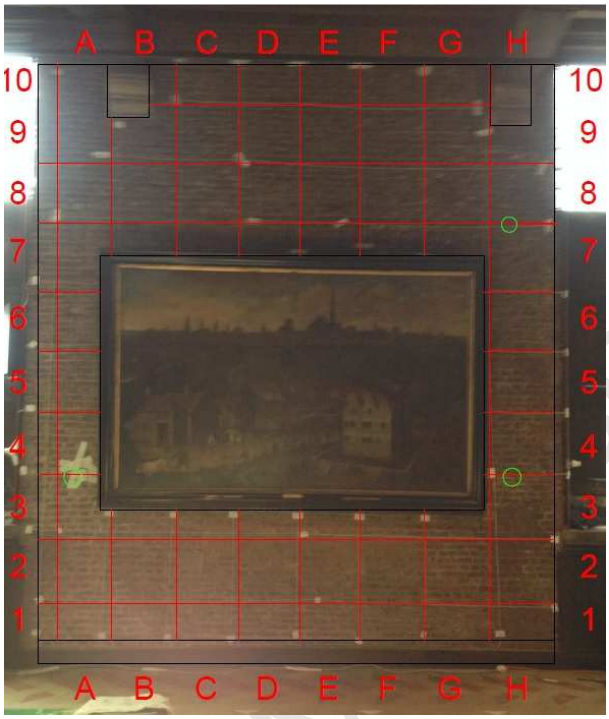

*Image 7.2.1; Wall section 1 grid surface (50*50 cm), grid distance from the floor level 50cm; the green points indicate the measurement points as described in Table 8.1.1*

*Image 7.2.2; Wall section 2 grid surface (50*50 cm), grid distance from the floor level 72cm; the green points indicate the measurement points as described in Table 8.1.1*

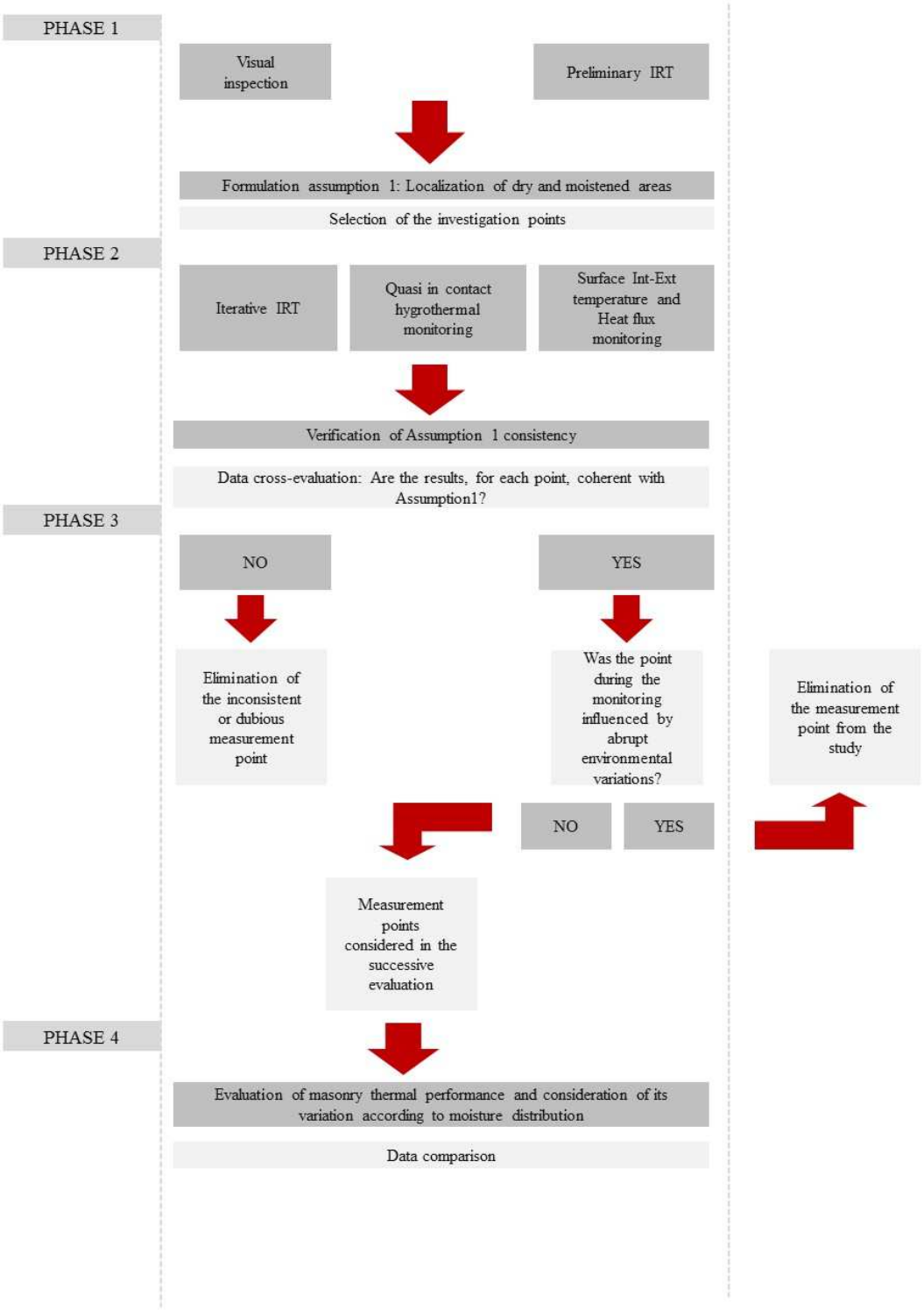

Image 7.2.3; Flow chart of monitoring activities

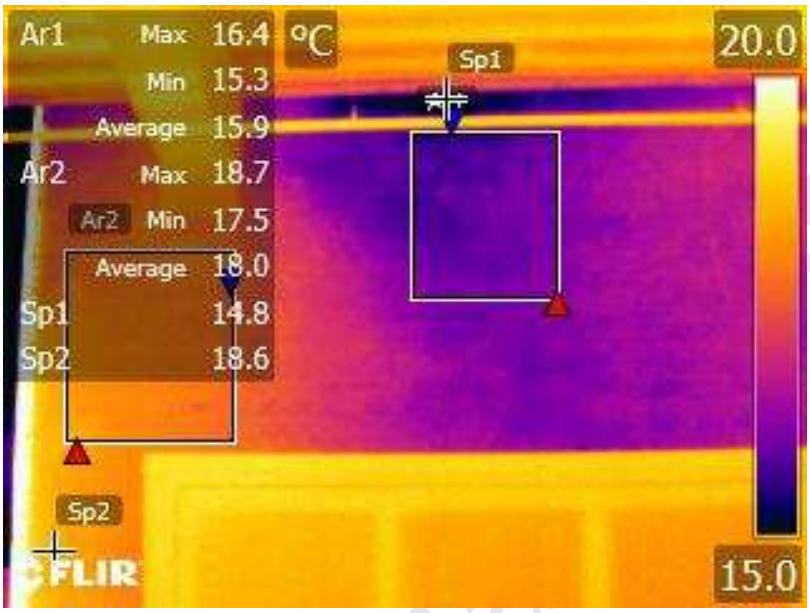

Image 8.1 1; Wall section 1; Left-top area; surface temperature gradient between the boxes positioned on both wet and dry areas; Spots temperature difference is proximity of the moistened and dry areas; Emissivity set at 0.93, brick red common- air temperature 20°C in Table 33.1 in [64]

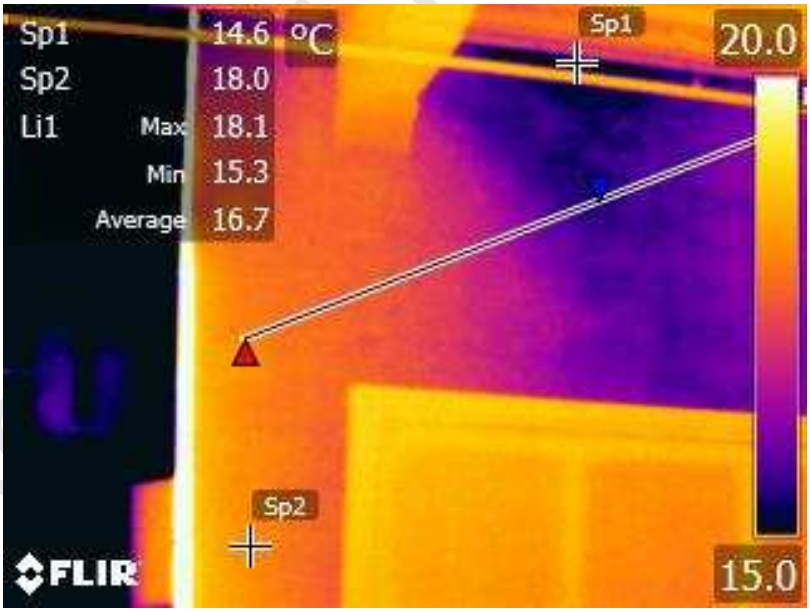

Image 8.1 2; Wall section 1; Central-top area; surface temperature gradient between the boxes positioned on both wet and dry area; Emissivity set at 0.93, brick red common, air temperature 20°C in Table 33.1 in [64]

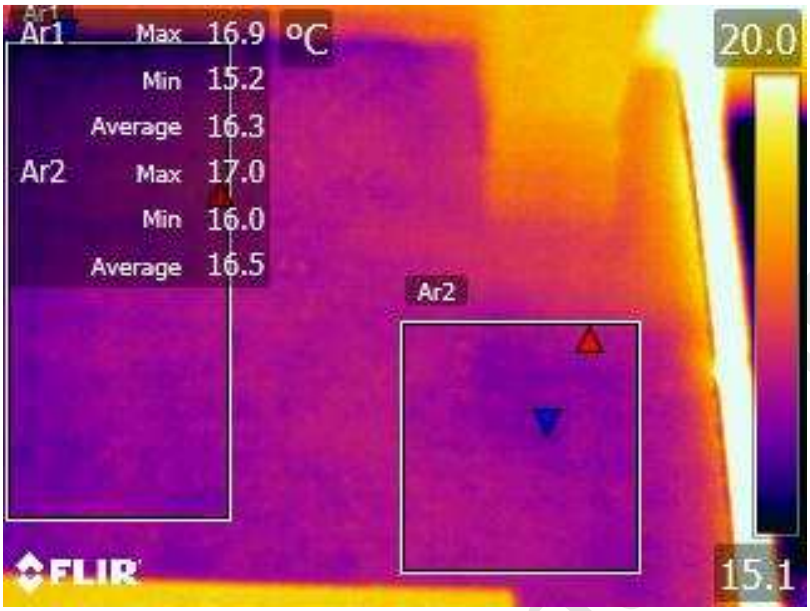

Image 8.1 3; Wall section 1; Central-right area; surface temperature gradient between the boxes positioned on both wet central area and wet right area; Emissivity set at 0.93, brick red common, air temperature 20°C in Table 33.1 in [64]

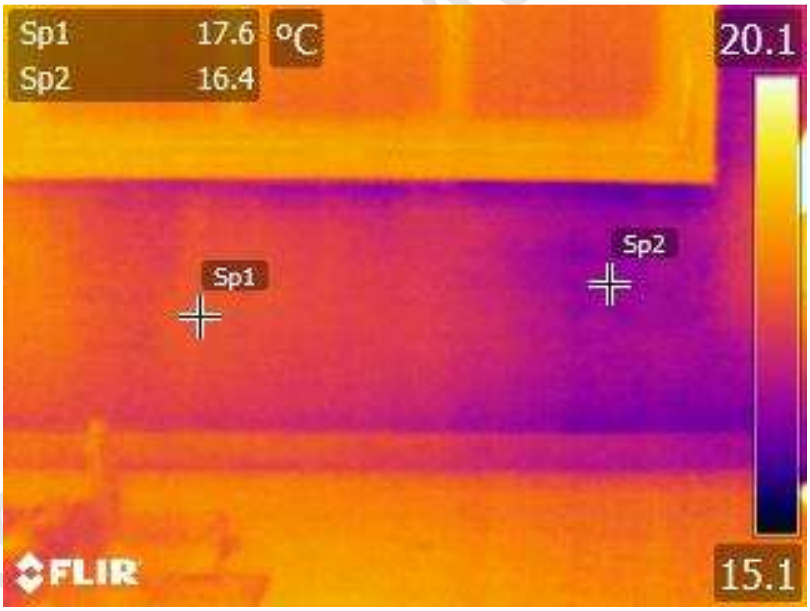

Image 8.1 4; Wall section 1; Right-bottom area; surface temperature gradient in proximity of the wall lower corner; Emissivity set at 0.93, brick red common- air temperature 20°C in Table 33.1 in [64]

Wall section	Point code	In contact measurement			Quasi in contact measurement							
		Heat Flow	Surface Temperature		Temperature		Relative Humidity		Mixing Ratio		Dew Point Temperature	
			Intern	Extern	Intern	Extern	Intern	Extern	Intern	Extern	Intern	Extern
1	A3	X	X	X	X	X	X	X	X	X	X	X
	H3	X	X	X	X	X	X	X	X	X	X	X
	H7	X	X	X	X	X	X	X	X	X	X	X
2	I7	X	X	X	X	X	X	X	X	X	X	X
	I5	X	X	X	X	X	X	X	X	X	X	X

Table 8.1.1; Measured quantities for each measurement point; In contact measured parameters: Heat flow (W/m^2); Surface Temperature (°C); Quasi in contact measured parameters (5mm distance from the wall surface): Relative Humidity (%); Mixing Ratio (g/Kg); Dew Point Temperature (°C)

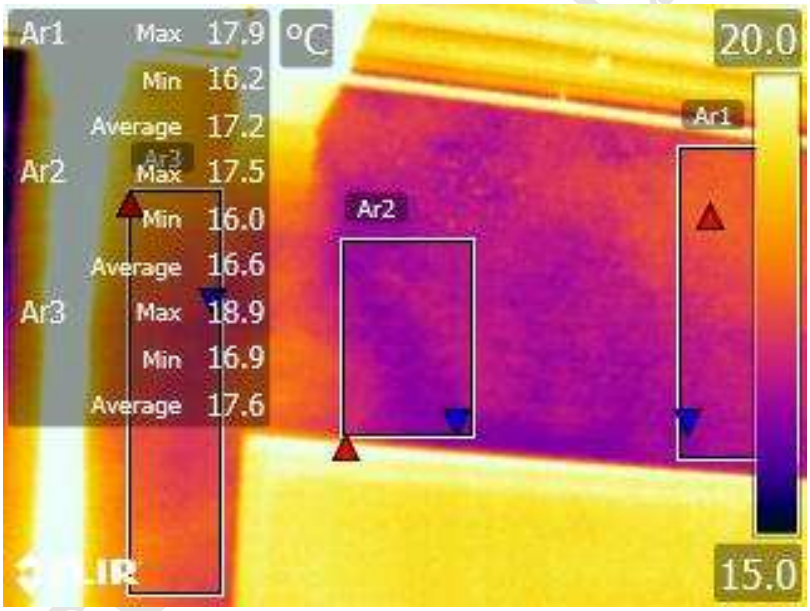

Image 8.1 5; Wall section 2; Central-top area; surface temperature gradient between the squares positioned on both wet and dry area; Emissivity set at 0.93, brick red common- air temperature 20°C in Table 33.1 in [64]

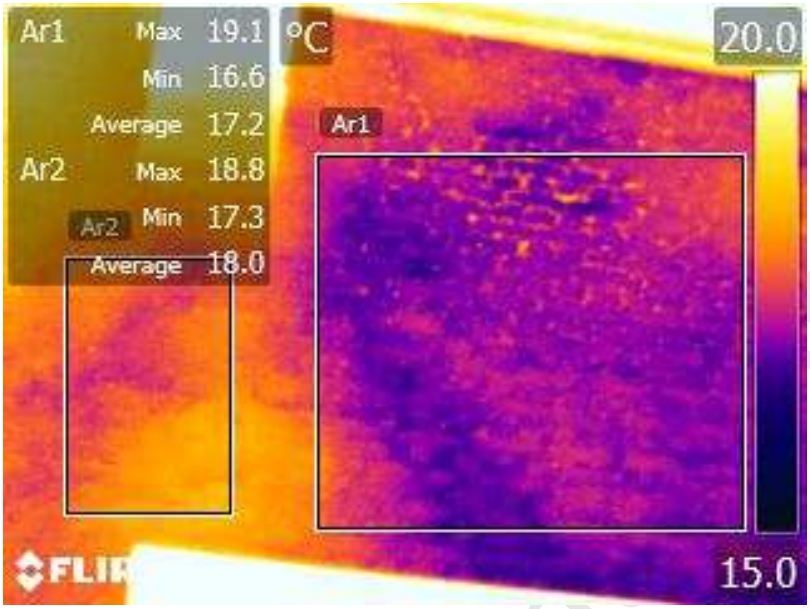

Image 8.1 6; Wall section 2; Central-top area; surface temperature gradient between the squares positioned on both wet and dry area; Emissivity set at 0.93, brick red common- air temperature 20°C in Table 33.1 in [64]

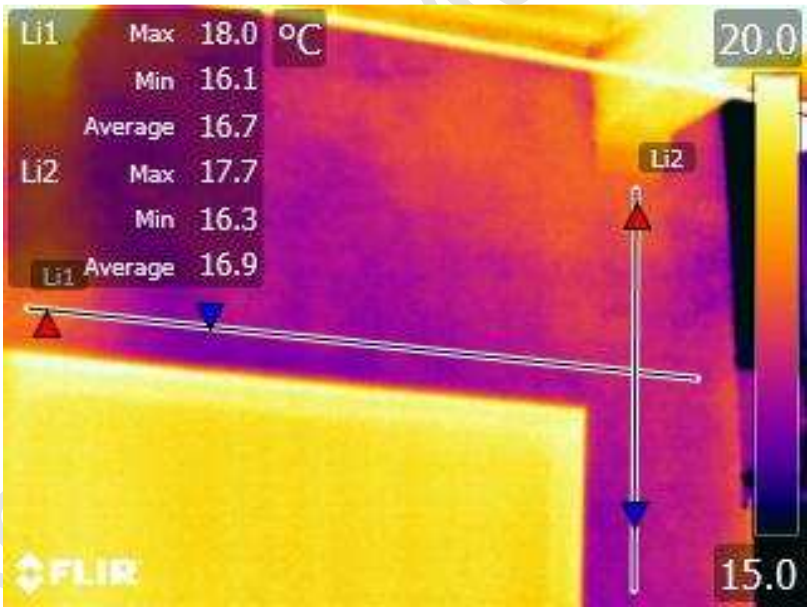

Image 8.1 7; Wall section 2; Right-top area; surface temperature gradient between vertical and horizontal line in proximity of the wall corner; Emissivity set at 0.93, brick red common- air temperature 20°C in Table 33.1 in [64]

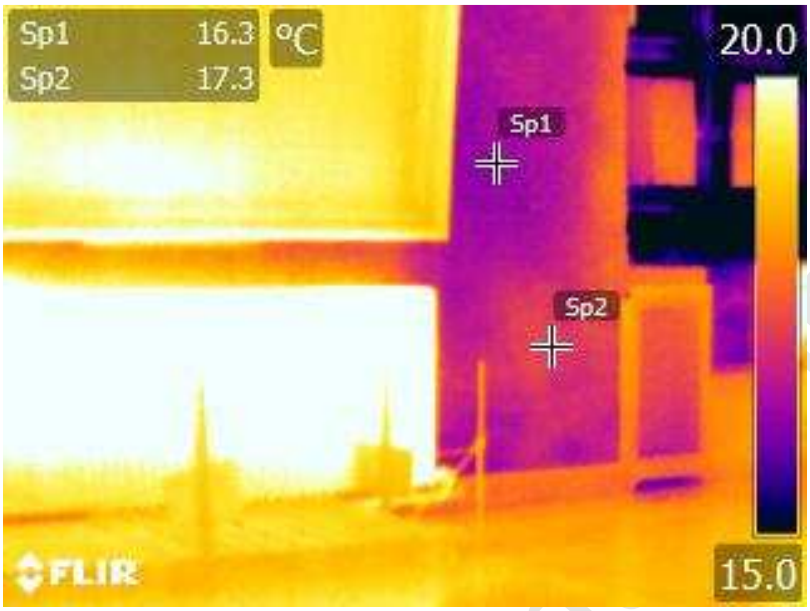

Image 8.1 8; Wall section 2; Right-bottom area; surface temperature different between two spots; Emissivity set at 0.93, brick red common- air temperature 20°C in Table 33.1 in [64]

	A	B	C	D	E	F	G	H
10	0.20	0.50	0.59	0.67	0.61	0.44	0.41	0.31
9		0.38	0.48	0.61	0.56	0.42	0.39	
8	0.19	0.33	0.41	0.47	0.53	0.41	0.56	0.45
7	0.16	0.31	0.38	0.44	0.50	0.44	0.44	0.42
6	0.19	NA	NA	NA	NA	NA	NA	0.41
5	0.19	NA	NA	NA	NA	NA	NA	0.23
4	0.20	NA	NA	NA	NA	NA	NA	0.44
3	0.17	0.28	0.39	0.38	0.41	0.55	0.56	0.36
2	0.16	0.25	0.33	0.33	0.38	0.44	0.53	0.36
1	0.27	0.31	0.34	0.38	0.41	0.47	0.50	0.41

Graph 8.2.1; Surface Temperature factor (μ_s^*) *in wall section I, March 7 2014*

θsmin	θsmax	σθs	Δ(θs-θsmin)	θiσ	σθe	Δ(θi-θe)	μsm	μs	μh	μs*	Time
16.3	19.6	18.11	1.81	20.6	14.2	6.4	0.33	0.61	1.73	0.39	15.20-16.36

Table 8.2.1; Data Summary; wall section I, March 7 2014

	A	B	C	D	E	F	G	H	I	J
10	NA	0.23	NA	0.47	0.45	0.41	0.41	0.39	NA	
9				0.52	0.47	0.41	0.36	0.36		
8	NA	0.36	0.44	0.50	0.48	0.48	0.47	0.45	0.28	NA
7	NA	0.41	0.30	0.59	0.58	0.55	0.55	0.50	0.45	NA
6	NA	0.42	NA	NA	NA	NA	NA	0.48	0.48	NA
5	NA	0.39	NA	NA	NA	NA	NA	0.58	0.48	NA
4	NA	0.39	NA	NA	NA	NA	NA	0.55	0.53	NA
3	NA	0.48	NA	NA	NA	NA	NA	0.61	0.48	0.39
2	0.09	0.42	NA	NA	NA	NA	NA	0.56	0.38	0.38
1	NA	0.42	NA	NA	NA	NA	NA	0.50	0.42	0.41

Graph 8.2.2; Surface Temperature factor (μ_s^*) *in wall section II, March 7 2014*

θsmin	θsmax	σθs	Δ(θs-θsmin)	θiσ	σθe	Δ(θi-θe)	μsm	μs	μh	μs*	Time
16.7	20	17.79	1.09	20.6	14.2	6.4	0.39	0.56	1.39	0.44	15.20-16.30

Table 8.2.2; Data Summary; *wall section II, March 7 2014*

	A	B	C	D	E	F	G	H
10	0.08	0.15	0.19	0.25	0.20	0.18	0.16	0.12
9		0.10	0.17	0.19	0.20	0.17	0.14	
8	0.07	0.09	0.13	0.15	0.17	0.18	0.18	0.21
7	0.06	0.08	0.13	0.13	0.16	0.19	0.18	0.18
6	0.05	NA	NA	NA	NA	NA	NA	0.17
5	0.04	NA	NA	NA	NA	NA	NA	0.15
4	0.04	NA	NA	NA	NA	NA	NA	0.17
3	0.08	0.15	0.14	0.15	0.14	0.17	0.19	0.10
2	0.07	0.11	0.11	0.11	0.13	0.17	0.19	0.12
1	0.10	0.14	0.11	0.11	0.12	0.15	0.17	0.15

Graph 8.2.3; Surface Temperature factor (μ_s^*) *in wall section I, April 14 2014*

θsmin	θsmax	σθs	Δ(θs-θsmin)	θiσ	σθe	Δ(θi-θe)	μsm	μs	μh	μs*	Time
19.7	22.6	21.27	1.57	22.33	11.52	10.81	0.76	0.90	2.49	0.10	10.00-11.30

Table 8.2.3; Data Summary; *wall section I, April 14 2014*

	A	B	C	D	E	F	G	H	I	J
10	NA	NA	0.07	0.16	0.20	0.19	0.14	0.12	NA	
9				0.20	0.24	0.19	0.12	0.09		
8	NA	0.07	0.05	0.22	0.22	0.25	0.15	0.13	0.12	NA
7	NA	0.05	0.01	0.15	0.19	0.19	0.19	0.17	0.15	NA
6	NA	0.04	NA	NA	NA	NA	NA	0.17	0.15	NA
5	NA	0.06	NA	NA	NA	NA	NA	0.18	0.16	NA
4	NA	0.09	NA	NA	NA	NA	NA	0.19	0.16	NA
3	NA	0.11	NA	NA	NA	NA	NA	0.19	0.15	0.13
2	0.06	0.06	NA	NA	NA	NA	NA	0.13	0.13	0.10
1	NA	-0.07	NA	NA	NA	NA	NA	0.11	0.11	0.10

Graph 8.2.4; Surface Temperature factor (μ_s^*) in wall section II, April 14 2014

θsmin	θsmax	σθs	Δ(θs-θsmin)	θiσ	σθe	Δ(θi-θe)	μsm	μs	μh	μs*	Time
19.6	23.1	20.91	1.31	22.33	11.52	10.81	0.75	0.87	1.93	0.13	10.00-11.30

Table 8.2.4; Data Summary; wall section II, April 14 2014

From Formula 5 in 6.1	Section I	Section II
(θi-θsmin) Percentage of reduction	38.84%	30.00%
(θi-θsi) Percentage of reduction	57.48%	49.71%

Table 8.2.5; Percentage of reduction on April 14th (compared to March 7th) of the Difference between Indoor air temperature and minimum surface temperature; and Indoor air temperature and mean surface temperature (See Formula 5 in 6.1)

	Mar-07	Apr-14
μ_d Section I	-0.93	-0.19
μ_{sm} Section I	0.33	0.76
μ_d Section II	-0.93	-0.19
μ_{sm} Section II	0.39	0.75

Table 8.2.6; Verification of surface condensation, See formula (3)

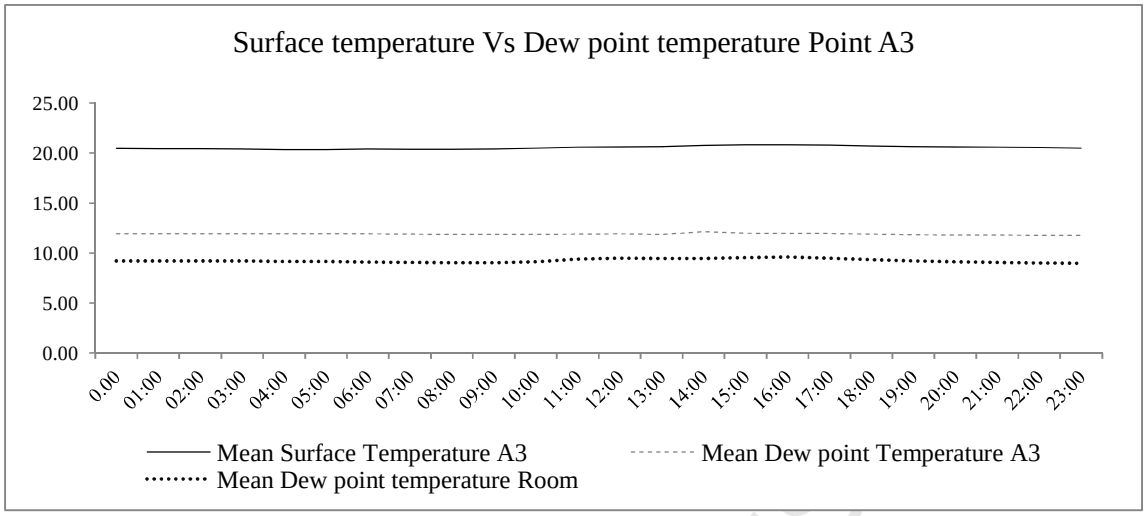

Graph 8.2.5; Surface Temperature vs dew point temperature evaluation; measured point A3

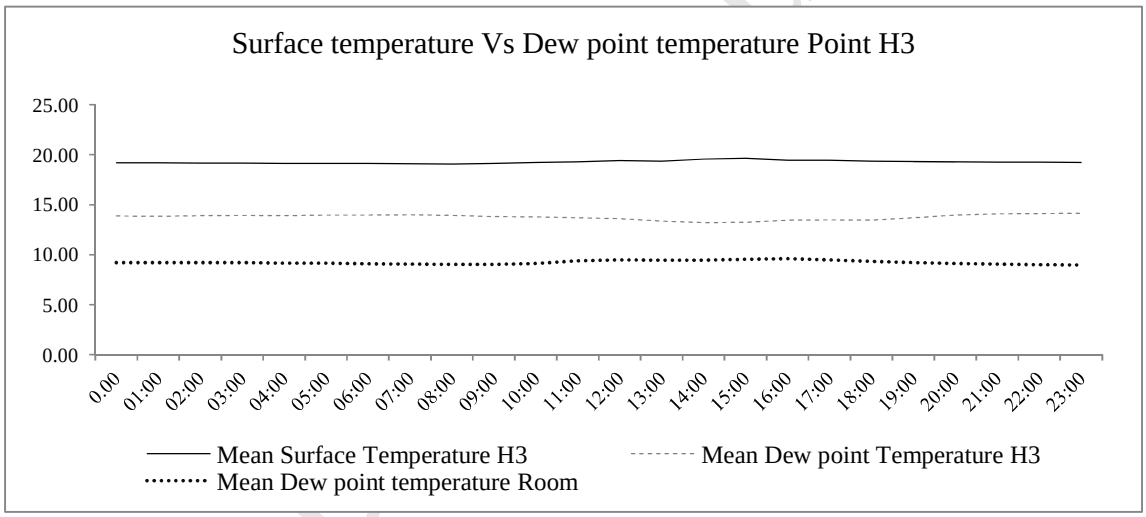

Graph 8.2.6; Surface Temperature vs dew point temperature evaluation; measured point H3

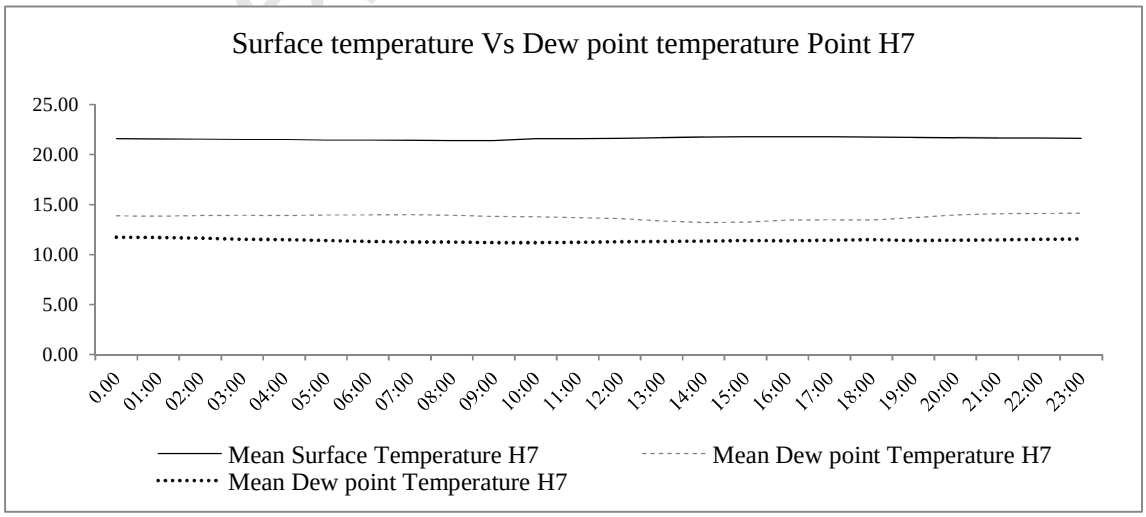

Graph 8.2.7; Surface Temperature vs dew point temperature evaluation; measured point H7

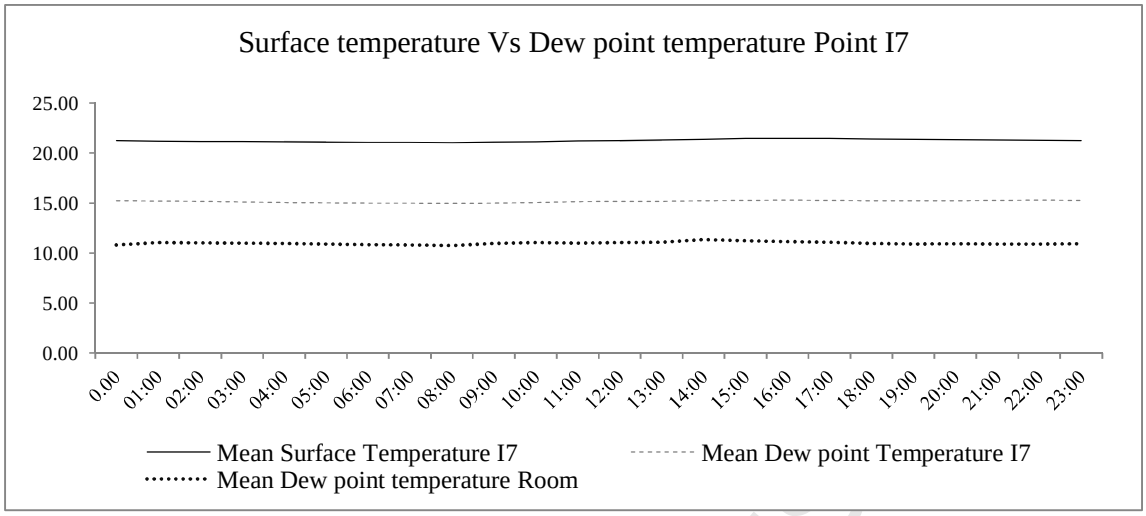

Graph 8.2.8; Surface Temperature vs dew point temperature evaluation; measured point I7

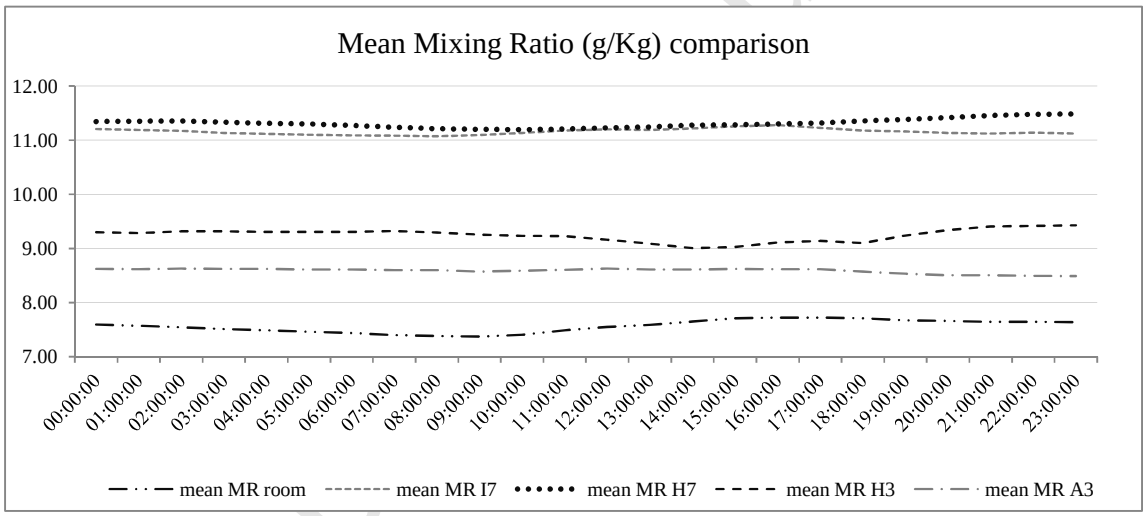

Graph 8.2.9; Mean Mixing Ratio (g/Kg) for the measured points

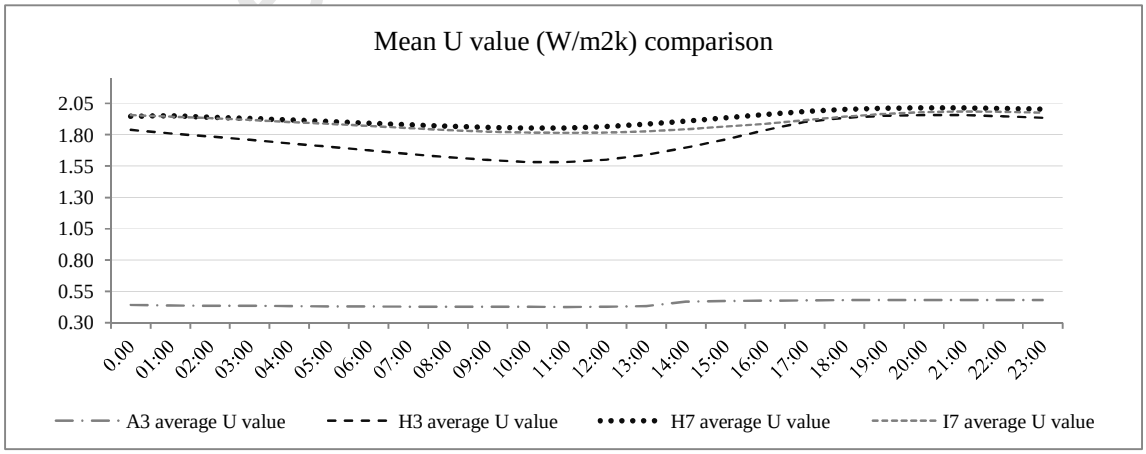

Graph 8.2.10; Mean thermal transmittance (W/m²K) for the measured points

	U (W/m²K) moving average method	U (W/m²K) matematichal average method	Deviation (%)
Point A3	0.478	0.428	10.47
Point H3	1.557	1.758	12.94
Point H7	1.586	1.933	21.87
Point I7	1.662	1.884	13.37

Table 8.2.7; Thermal transmittance value (W/m²K) point deviation between mathematical average method and mean moving average method.

Measurement Point	Indoor Surface Temperature, Standard Deviation	Outdoor Surface Temperature, Standard Deviation	Heat Flow, Standard Deviation	Thermal conductance (Λ) uncertainty (W/m²K)
A3	0.14	0.56	0.56	±0.08
H3	0.44	1.64	0.64	±0.83
H7	0.77	1.97	1.19	±1.04
I7	0.21	0.86	0.46	±0.45

Table 8.2.8; Uncertainty evaluation per measurement point; independent variables (indoor-outdoor surface temperature and heat flow) standard deviation; measured thermal conductance (Λ) uncertainty.

Highlights:

- Proposal of indirect assessment methodology for hygrothermal evaluation of traditional masonry
- Iterative Infrared thermography, Heat flow and hygrothermal monitoring for walls hygrothermal diagnosis
- Moisture influence evaluation on thermal performance of traditional masonry in heritage buildings
- Thermal transmittance and heterogeneity surface temperature factor increase due to localized residual moisture